REPORT ON NEUTRAL PARTICLE DETECTORS AND QED

PEP SUMMER STUDY

August, 1974

E. D. Bloom, F. Bulos, G. Buschhorn, J. Dakin, E. B. Hughes,
T. Mast, J. Nelson, A. Odian, C. Prescott, S. Yellin, D. Yount

ABSTRACT

The exploration of the neutral particle final states in e^+e^- annihilation using a 4π neutral particle detector is discussed. Charge particle final state physics is also considered in the context of a neutral detector. Design criteria are discussed, and a possible detector design is presented.

Edited by: E. D. Bloom
E. B. Hughes

INDEX

I INTRODUCTION

One area of e^+e^- colliding beam physics which has only been sparsely explored to date is the study of neutral particle production in e^+e^- hadrons. Results from the magnetic detector at SPEAR have tantalized us,[1] but a comprehensive picture is yet to emerge. In the view of the participants of this study (Neutral Detectors II), there seems to be a strong need at PEP for a detector complementary in concept to the large solid angle magnetic detector. The most important attributes that this "neutral detector" should possess are 1) essentially 4π (>98%) solid angle acceptance and 2) excellent energy and position resolution for γ's with energies ranging from the maximum possible down to the vicinity of 50 MeV. The neutral detector would not ignore charged hadrons, but its objectives would be achieved at the expense of a magnet for charged hadron momentum measurement. Instead, emphasis is placed on the construction of a compact, precision, γ-ray detector located as close as possible to the interaction region. Tracking chambers and hadron calorimetry would be used to obtain multiplicity and energy information on the charged hadron component of the final state and to provide, in addition, information on those neutral hadrons which do not decay into γ's. Unlike the large solid angle magnetic detector which measures charged particles well and γ-rays not so well, the large aperture neutral detector would measure γ-rays well and both charged and neutral hadrons not so well.

Specifically, the areas of physics that can be explored with the detector outlined above are as follows:

a) the measurement of the total cross section for $e^+e^- \rightarrow$ hadrons (the use of a total energy measurement in the trigger for such events is very attractive, since several sources of bias are removed[2]);

b) the measurement of the γ, π^o and η^o inclusive cross sections, total hadron multiplicities and hadron correlations;

c) the study of QED through the reactions $e^+e^- \rightarrow \gamma\gamma$ and $e^+e^- \rightarrow e^+e^-$ ($e^+e^- \rightarrow \mu^+\mu^-$ could also be measured by including the appropriate magnetized μ filters);

d) the measurement of the total cross section for $e^+e^- \rightarrow e^+e^-$ + hadrons (this reaction can be recognized both by a total energy measurement and through the use of tagging counters);

e) the search for new particles (given the large solid angle and the ability to recognize electrons, γ's and muons).

Also, the search for evidence of weak neutral currents in the reaction $e^+e^- \rightarrow \mu^+\mu^-$ might be attempted. The detection of this reaction in the range $40^o < \theta < 140^o$ with $\Delta\phi = 2\pi$, provides good sensitivity to the expected charge asymmetry due to interference between the neutral weak and electromagnetic currents[3].

In the following sections the principal physics areas (items a-e above) accessible to a large solid angle "neutral" detection apparatus are discussed in more detail. Appendix I contains one possible design for such a detector, together with interaction region requirements and a cost estimate. A useful summary of properties of presently available detectors for γ-rays can be found in the Proceedings (PEP-155).

II $e^+e^- \rightarrow$ Hadrons

A number of aspects of the reaction

$$e^+e^- \rightarrow \text{hadrons} \tag{1}$$

can be accurately studied with an apparatus capable of large solid angle, track-vertex information, precise and efficient photon detection, and hadron calorimetry (such as that described in Appendix I). For the purpose of this discussion we will consider two extreme models of how reaction (1) might proceed at PEP energies. In both models we assume that the hadronic final states contain only pions, and that the average multiplicities $\langle N_{\pi^+} \rangle$, $\langle N_{\pi^0} \rangle$ and $\langle N_{\pi^-} \rangle$ are equal. In Model I, the "hard-π" model, we assume that the inclusive cross section for $e^+e^- \rightarrow \pi +$ hadrons scales as

$$s \frac{d\sigma}{dx} = 1.4 \times 10^4 \; e^{-7.24x} \text{ nb GeV}^2 \tag{2}$$

Here s is the total c.m. energy squared, and x is the c.m. π energy divided by $\sqrt{s}/2$. In Model II, the "soft-π" model, we assume the inclusive cross section scales as

$$\frac{1}{\sqrt{s}} \frac{d\sigma}{dp} = 1.3 \times 10^2 \, p \, e^{-3.76p} \text{ nb GeV}^{-3} \tag{3}$$

Here p is the π c.m. momentum. Model I produces Bjorken scaling; Model II produces a constant total cross section and a universal π c.m. momentum distribution. Both models are properly normalized to agree with the data from SPEAR-I at $s = 25$ GeV^2.[1,4] The implications of each model for PEP at $s = 900$ GeV^2 are summarized in Table I. The integral cross sections for inclusive π^0 and γ production are given in Figs. 1 and 2 respectively.

Reaction (1) can be identified by requiring two charged particles from the interaction region and a total final state energy of $\gtrsim 15$ GeV. Few events are excluded by the 2-charged particle requirement. We estimate that $< 1\%$ will be lost due to geometric inefficiency and that $\lesssim 5\%$ of the multi-hadronic final states contain no charged particles[2]. The total final state energy E_{tot} can be measured in two independent ways. The first is to sum the neutral energy from the inner detector and the hadron energy from the calorimeter (which surrounds the inner detector). Here we expect to measure the "γ" energy to $< \pm 1\%$, and the "non-γ" energy to $\lesssim \pm 30\%$[5]. Hence, E_{tot} will be measured with a typical accuracy of $\lesssim \pm 20\%$. The second method does not require charged hadron calorimetry but is based instead on the assumption that the average π^o, π^+ and π^- energies are the same in a given event. This assumption presumably improves with increasing multiplicity. One can measure the number of π^o's and the average π^o energy with the inner detector. Then, assuming that each of the charged prongs has this same energy, one can calculate the assumed total energy. The results of a study of this method are shown in Fig. 3. For this study, multi-pion final states were selected by a phase-space Monte Carlo program. The average total multiplicity was chosen to be 15, approximately that of Model I. The total c.m. energy was set at 30 GeV. When the above energy algorithm was applied to the multi-pion final states, the estimated total energy, E_{tot}, was less than 15 GeV with only 8% probability. The "resolution" of this energy algorithm is seen to be $\pm 33\%$, somewhat worse than the resolution of the calorimetry.

The requirement of two charged prongs and $E_{tot} > 15$ GeV may include some backgrounds to process 1. We will briefly mention these and their

treatment. The processes $e^+e^- \rightarrow e^+e^-$ and $e^+e^- \rightarrow \mu^+\mu^-$ are easily recognized and are used to test QED, as discussed in Section IV. Beam-gas processes can be understood through their typically low E_{tot} and $p_\perp$ and the fact that their verticies do not cluster in the luminous region. The cross section for the 2-photon annihilation process $e^+e^- \rightarrow e^+e^-$ + hadrons to produce an hadronic final state of invariant mass $3.0 < M_x < 10$ GeV is estimated to be $0.2 \times 10^{-33} cm^2$ [6]. This cross section is comparable to the cross section for $e^+e^- \rightarrow$ hadrons. ($0.45 \times 10^{-33} cm^2$ for Model 1.) However, a number of characteristic features of the 2-photon process will allow its study and subsequent removal from the reaction 1 data sample. Among these are: 1) the fact that we will detect and identify at least one of the final state e's at $\theta > 14$ mrad 30% of the time; 2) the expected longitudinal momentum asymmetry; 3) the expected low transverse momenta; and 4) the low characteristic E_{tot}. Indeed, using E_{tot}, one may be able to measure $\sigma_{tot}^{\gamma\gamma}$, see Fig. 4.

To measure σ_{tot} for reaction 1 we will identify events using the above trigger scheme. The number of events will be normalized to the luminosity monitors discussed in Section IV. Corrections will be applied for the effects described above and summarized in Table 2. We estimate that the dominant uncertainty will be in the correction for the 2-photon process.

We can easily measure some of the global properties of the multihadronic final state once the events of reaction 1 have been identified. By counting prongs we can measure the average charged multiplicity. By summing the pulse heights from the counters (which don't have charged prongs entering them) we can measure the fraction of $\sqrt{s}$ going into neutral particle energy. For both of these measurements, as for σ_{tot}, the large solid angle of the apparatus and the "energy trigger" allow a result which is largely model independent.

By detecting the individual photons in the multi-hadronic final states, a great deal can be learned without reconstructing individual π^o's. Assume that all γ's come from π^o decay and that we measure the inclusive cross section for

$$e^+e^- \rightarrow \gamma + \text{Hadrons} \quad (\text{and } \gamma\text{'s}). \tag{4}$$

This is possible because the inner detector will detect γ's over the energy range ~ 10 MeV $< E_\gamma \leq 15$ GeV, with excellent energy resolution[7] (FWHM $\sim 2/E[\text{GeV}]^{1/4}$%). Furthermore, the counting rates are ample. As shown in Fig. 2, for either model there are ~ 100 γ's/hour for $E_\gamma > 1.7$ GeV. The rate falls to less than 1 γ/hour for $E_\gamma > 3$ GeV (Model II) or $E_\gamma > 9$ GeV (Model I).[15]

Two important features of the parent π^o inclusive spectrum can be found directly from the γ inclusive spectrum. First, for $E_\gamma \gg m_\pi$, the γ angular distribution gives the parent π^o distribution. One can easily distinguish between a uniform and a $(1 + \cos^2\theta)$ distribution. Second, the scaling properties of the γ inclusive cross section reflect the scaling properties of the parent π^o distribution. If, for instance $s\frac{d\sigma}{dx}$ scales for the π^o's, as in Model I, then it will also scale for the γ's.

Another interesting question is whether there is any direct γ production in reaction 1. It will probably not be possible to tell whether a given γ is or is not a decay product of a neutral hadron, because we cannot detect and pair all of the γ's in every event even if they do all come from π^o's and η^o's. This is because the soft γ's from asymmetric π^o decays are particularly difficult to handle (see Section IV). Statistically, however, we can hope to reconstruct the π^o and η^o spectra, and hence that component of the γ spectrum due to π^o and η^o decay. Then a subtraction will show whether there is an excess of directly-produced γ's.

III $e^+ + e^- \rightarrow \pi^o$ + Anything

Here we report the results of a Monte Carlo study which attempts to reproduce the experimental situation. Neutral pions are detected by observing photons from the 2γ decay. Other decay modes are ignored. The purpose of this study is to determine the influence of spatial resolution, energy resolution, and energy threshold on the pion identification efficiency. A confusion can arise from the presence of other photons in the final state of an event. This confusion is studied by taking a multi-pion final state for consideration. In some cases studied here, soft photons are also included to simulate the presence of background photons from beam spray, bremsstrahlung, and other unwanted processes.

Neutral pions are chosen from one of two distributions. The first, called "Model 1", corresponds to assuming that particle spectra at PEP will scale in $x = E/E_o$. Fitting present SPEAR data to an exponential yields[1,4]

$$dN/dx = A \exp(-7.24x) \qquad \text{Model 1 ("hard-}\pi\text{" Model)}$$

If one assumes that particle multiplicities increase with s, but the momentum spectrum is unchanged, a fit to present SPEAR charged particle data yields[1,4] the second distribution.

$$dN/dx = A\, p \exp(-3.76\, p) \qquad \text{Model II ("soft-}\pi\text{" Model)}$$

The first model is a "hard pion" model because of production of relatively high energy pions. The second is a "soft pion" model because of the predominantly low energy pions it produces.

a) Photon Generation

Neutral pions are chosen from one of the two models described above with a multiplicity of 10 π^o's, intermediate between Models I and II. This is chosen to adequately represent the confusion arising from multiple photons.

Pions are distributed isotropically in space. Correlations between pions and conservation of momentum are ignored. All π^o's decay isotropically in its center-of-mass system, yielding 20 photons in space. Each photon has its spatial position and energy randomly adjusted according to resolution functions of the device. If the energy of the photon falls below the energy threshold of the counter, the photon is removed from consideration. Each photon is tagged with an index from the parent π^o for later bookkeeping purposes. Detection of photons is accomplished in a shower counter. The resolution in energy and angle for the photons detection depends upon the type of counter used. Also the ability to detect low energy photons differs in different counters.

Two types of counter devices are considered here:

a) A NaI(Tl) detector - its resolution parameters are

(1) $dE/E = 0.02/E^{1/4}$ (FWHM)

(2) E-threshold = 10 MeV

(3) $dx = \max(.1, .18/E^{.65})$ cm., E in GeV ($\frac{1}{2}$ FWHM)

b) A Pb Glass detector - its parameters are

(1) $dE/E = 0.10/E^{1/2}$ (FWHM)

(2) E-threshold = 40 MeV

(3) $dx = \max(.1, .18/E^{.65})$ cm., E in GeV ($\frac{1}{2}$ FWHM)

Thus for a 100 MeV photon dx = 0.8 cm for both NaI(Tl) and Pb glass.

The spatial resolutions used here are those suggested in a report by T. Mast and J. Nelson (see PEP-153) for converting photons in 2 r.l. active converters, on the basis of a Monte Carlo study of showers. The conversion probability for photons is not included in the present study. It depends on the energy of the photon and on the design of the active converters. Since the converters are backed up by large segmented counters the position resolution for the photons which do not convert is considerably broadened ($\sim \pm 5^o$) but the energy resolution is unaffected.

The details of how photon conversion inefficiency modifies the results contained in this report depend critically on the design parameters of the photon converters. These inefficiencies are ignored at the present, but can be incorporated later, once the inefficiencies have been measured or calculated for the converters.

A 5^{o} cone is allowed for beam pipes; photons falling within 5^{o} of the forward or backward directions ($\Delta\Omega/4\pi = 0.4\%$) are removed. For the cases where two photons fall within a distance of 2 dx of each other, one is removed and the other is given the sum of the two energies. Finally, where indicated, background photons generated from a "soft" spectrum (arbitrarily chosen to be dn/dE = A exp (-E/.1), E in GeV),are distributed isotropically. The array of observed photons are then passed to a pion-finding algorithm.

b) The Pion Identification Algorithm

From the array of n photons n(n-1)/2 photon pairs are considered. Each pair defines an invariant mass. High energy photons (with energy greater than that for a pion whose half-opening angle cannot be resolved) are called π^{o}'s and are removed from further consideration. Next, two photon pairs are considered. Each pair combination is assigned a probability P_1 which represents the probability of measuring a value M^2 different from m^2_π with a resolution dM^2. A normalized gaussian probability is used here. In addition a probability P is assigned which represents the probability $p_2(E,\theta_{\gamma\gamma})$ for two photons from a pion of energy E to have an opening angle $\theta_{\gamma\gamma}$. This distribution is singular at $\theta = \theta_{min}$, until counter resolution is considered. Below θ_{min}, a gaussian distribution of width given by the angular resolution is used. Each two photon pair is assigned a probability $P_1 * P_2$. The array of two photon pairs is searched for the maximum probability. That pair is

taken as the first π^o, and all other pairs which use either of the two photons are removed from further consideration. Then a second two-photon pair is chosen from the remaining combinations, having the highest remaining probability, and so forth until no pairs remain. The resulting π^o's are called identified π^o's. Some are correctly identified, and some are wrongly paired. Since the photons are tagged with the parent pion, the efficiency of correct pion identification can be determined. This is the identification efficiency plotted in Figs. 8-10.

c) Results

(i) Figure 5 shows the photon energy spectrum from the two models, I and II. The spectra peak at low photon energies, around 70 MeV. Below this energy they drop rapidly to 0. Below 50 MeV there are approximately 10 percent of the photons for both Model I and Model II. Clearly, efficient pion identification requires good low energy response for a shower detector.

(ii) Figure 6 shows the invariant two photon mass squared distribution for NaI(Tl). All two photon combinations are shown. Most of these do not survive the algorithm. Of those which do, there are two categories: correctly identified photon pairs, and incorrectly paired photons. The mass spectra for these two cases are also shown.

(iii) Figure 7 shows the ability to separate π^o from η^o for NaI(Tl).

(iv) Figure 8 shows the pion identification efficiency vs E_π for NaI(Tl) and Pb Glass (PbG) counters for the Model I pion spectrum. Here the influence of additional random background photons is also considered.

(v) Figure 9 shows the dependence of efficiency on the number of pions per event, for both Model I and Model II, for NaI(Tl) and Pb Glass type counters.

(vi) Figure 10 shows the dependence of efficiency on the number of background soft photons. Here the efficiency is averaged over the pion spectra.

(d) Discussion and Conclusions

The primary purpose of this study is to determine the ability of NaI(Tl) and Pb glass type shower detectors to see π^o's in a multiple π^o final state. A final state of 10 π^o's has been chosen to represent a typical event at 30 GeV c.m. Two pion spectra are used: a "soft" pion spectrum (Model I) and a "hard" pion spectrum (Model II). High efficiency requires the identification of many soft photons. Identification of π^o's is done with an algorithm described in the text. The identification efficiency is defined to be the ratio of correctly paired photons into π^o's to the total in the sample of π^o's. This efficiency clearly depends on the algorithm used (as well as on the detector resolution parameters) and it's likely that other algorithms or techniques may prove to be better. The efficiency increases with E_π, reaching 95% for NaI(Tl) at E = 2 GeV and 87% for Pb Glass at 2 GeV. At lower energies the NaI(Tl) drops to 83% at 0.2 GeV, while the efficiency for Pb Glass drops below 50%. The lower efficiency for Pb Glass relative to NaI(Tl) is primarily due to its poorer energy resolution, since the spatial resolution is assumed to be the same in both cases. The higher threshold used for Pb Glass contributes only 6% to the inefficiency because the single photon energy spectrum falls rapidly to 0 below 70 MeV. The multiplicity of the final state affects the efficiency seriously. For a 14 π^o final state of soft pions (Model II) NaI(Tl) will be 75% efficient while Pb Glass falls below 40%, averaged over the spectrum. Inefficiencies due to lack of conversion of soft photons in the active converters have not been included yet. Once

these effects have been measured or calculated they can easily be folded into the results. Finally, background soft photons also lower the efficiency, typically 10% for 10 extra photons per event. Clearly careful attention to background spray is important to the clean identification of π^o's in a large solid angle shower counter.

IV QED at PEP

(a) General

It is inevitable that QED will be tested in several detection systems at PEP. (A brief reference to event rates and sensitivity to cut-off parameters is included in Appendix IV). Certainly a large aperture magnetic detector will be able to measure the angular distribution in Bhabha scattering in the range $40^o<\theta<140^o$ and the relative rate of $e^+e^- \to \mu^+\mu^-$ (as in experiment SP-2 at SPEAR-I). Probably a large aperture non-magnetic detector (such as that described in Appendix I) will be able to measure the angular distributions in $e^+e^- \to \gamma\gamma$ and $e^+e^- \to e^+e^-$ also in the range $40^o< \theta < 140^o$.

It is doubtful that such detectors will significantly augment their ability to test QED in Bhabha scattering and $e^+e^- \to \gamma\gamma$ by making use of events detected at smaller angles ($10^o<\theta<40^o$): a) because the q^2 values for the dominant diagrams are small, and b) because the rapid angular dependence of the cross section in this range makes unbiased measurements difficult. A much better approach is to operate such detectors in conjunction with precision luminosity monitors. It should also be remembered that q^2 values equal to those available in the angular range $10^o<\theta<40^o$ at a machine energy of 15 GeV are also available at PEP in the range $40^o<\theta<140^o$ at a machine energy of 5 GeV. This means that even if the measurements on

Bhabha scattering and $e^+e^- \rightarrow \gamma\gamma$ are confined to $40^\circ<\theta<140^\circ$, it will still be possible to make measurements at q^2 values equal to the maximum available at SPEAR-II by operating PEP at energies down to 5 GeV. If a violation of QED is discovered at PEP energies, it will be very important to verify in the same experiment that QED is not violated at the maximum q^2 values accessible to SPEAR-II (assuming, of course, that QED is valid at SPEAR-II).

Any detector intended to make measurements of the precision and clarity needed to test QED exhaustively at PEP energies should be able to verify that the total center of mass energy is present in the detected final state and should be able to measure with precision the energy, coplanarity and collinearity distributions of the outgoing particles. It will then be possible to compare each of these distributions with the QED prediction. This type of detector will need to measure γ-ray directions precisely and be able to recognize or eliminate contributions to the measured distributions from $e^+e^- \rightarrow e^+e^-e^+e^-$ and $e^+e^- \rightarrow e^+e^-\mu^+\mu^-$, both of which have large cross sections at PEP energies.

(b) Considerations Affecting the Design of a Luminosity Monitor for PEP.

There appear to be no reasons why a small angle Bhabha scattering luminosity monitor, of the type originally proposed by Barbiellini, et al,[8] and since used successfully at Adone and at SPEAR-I (in experiment SP-4), cannot also be used at PEP. A luminosity monitor at PEP, viewing the luminous region at $\sim 4^\circ$, as in SP-4, would detect Bhabha scattering for space-like $q^2 = 1.1$ GeV^2. Experiments at CEA and SPEAR-I have shown that the space-like photon propagator is within a few percent of the QED value for $q^2 \simeq 10$ GeV^2. It is, therefore, a conservative assumption that the Bhabha cross section in a 4° monitor at PEP can be calculated according to standard

QED, and the motivation to go to smaller angles is weak. Moreover, 4^{o} is comfortably large compared to the expected angular divergence of the beams in the luminous region at PEP ($\leqq$1 mr). Precision luminosity monitors at much smaller angles would be troubled by corrections necessary to acccount for the larger proportional uncertainties in the true scattering angles.

Preliminary calculations, based on the work of Berends, et al,[9] indicate that the radiative corrections, computed to order α^3, remain moderate (~5%) at 15 GeV for a monitor essentially identical to the one used in SP-4. If order α^3 corrections remain adequate at PEP energies, there should be no problem in computing them to better than $\pm$ 1%.

The SP-4 monitor occupied an overall length of about 4 meters, much less than any pit length being considered for PEP. The counter telescopes themselves were about 8 inches in overall length, and they do not need to be significantly larger at PEP. Thus, monitor design considerations put no firm constraints on the pit length. Nevertheless, given the existence of a 10 or 20 meter pit, utilizing the full length by simply scaling up the linear dimensions of all parts of the SP-4 monitor would offer a number of modest advantages. These are:

1) Experience at SPEAR-1 indicates that all background arrives in prompt time with the circulating bunches. A time of flight of 30-60 nanoseconds between the two ends of the pit would make it easy to time out that part of the background approaching each counter from the side away from the interaction region. Such background is invariably soft and incapable of triggering the shower (energy threshold) counters, but it can be an annoying source of accidentals in the plastic telescope counters when the energy threshold is exceeded by a true Bhabha event outside the small defining plastic counter aperture but within the larger shower counter aperture.

2) The larger overall size of all the detectors would make it possible to replace lead-plastic scintillator shower counters with NaI(Tl) so that the good inherent energy resolution of the latter detector could be obtained. This might or might not be useful in rejecting certain kinds of spurious events, depending upon the nature of the background environment. In any case, the detailed shape of the energy spectrum in small angle counters is of some intrinsic interest as a check on the adequacy of the calculation of the radiative correction, which can predict the energy spectrum.

3) The larger linear scale of the PEP monitor would reduce the tolerances on the absolute positions and sizes of the defining counters. These tolerances were quite severe for the 4 meter long monitor in SP-4.

Double bremsstrahlung monitors at PEP appear to be very unattractive due to the very high backgrounds from single bremsstrahlung. A corroborative precision monitor, based upon a physical process other than Bhabha scattering and with its own radiative corrections, would provide a convincing check on a Bhabha monitor. One possibility is the detection of $e^+e^- \to e^+e^-e^+e^-$, but only if an efficient tagging system can be set up at very small forward angles.

(c) Detector Design

The following remarks refer principally to the design of a non-magnetic detection apparatus for the precise measurement of $e^+e^- \to \gamma\gamma$. This detector will almost automatically be able to make precise measurements on Bhabha scattering and should be surrounded by a large aperture muon filter, plus track chambers, to detect $e^+e^- \to \mu^+\mu^-$. The acceptance in polar angle should be large and no less than $40^\circ<\theta<140^\circ$. The acceptance in azimuth should be large and also symmetric in order to make the total response independent of transverse beam polarization. The muon filter

should be of magnetized iron in order to distinguish muons with the full beam energy from those produced by the background process $e^+e^- \rightarrow e^+e^-\mu^+\mu^-$.

The energies of electrons and γ-rays are best defined by NaI(Tl) detectors. These detectors will probably consist of arrays of NaI(Tl) modules. Each module may be hexagonal in cross section, about 25 sq. in. in acceptance area and no less than 14 inches deep. The available energy resolution should be at least as good as $\text{FWHM}(\%) = 2.0/E(\text{GeV})^{1/4}$. Pb Glass can be substituted for NaI(Tl) only at the expense of a substantial loss in energy resolution. Calculations show that composite detectors consisting of NaI(Tl) converters followed by Pb glass absorbers have energy resolutions that are very strong functions of the thickness of NaI(Tl) until this thickness exceeds about 10 radiation lengths. This means that a sensible choice of detector is reduced to either all NaI(Tl) or all Pb glass.

The directions of electrons will be defined by track chambers located upstream of any γ-ray converters. The γ-ray converter design should be chosen in order to optimize conversion efficiency, directionality and energy resolution. "Live" NaI(Tl) converters will be necessary if the total converter thickness is greater than about 1 radiation length. If a very large conversion efficiency is required, it may be necessary to use multiple converters, each of thickness 1 radiation length.

In SPEAR experiment SP-4, a single "dead" converter (1.1 radiation length of lead) was used, followed by a 7 in. drift space occupied by track chambers. This converter design degraded the γ-ray energy resolution by less a factor of about 1.5 (relative to a live NaI(Tl) converter), provided good conversion efficiency, gave good γ-ray directionality, and avoided the use of multiple converters. This design could be used at PEP for $e^+e^- \rightarrow \gamma\gamma$, but if lower energy γ-rays from π^o decay are to be detected simultaneously

it may be desirable to increase the total converter thickness (efficiency) without losing energy resolution, directionality (for $e^+e^- \rightarrow \gamma\gamma$), and without unduly increasing the detector volume (multiple drift spaces are unattractive). Multiple live converter designs (without drift space) will be possible if the γ-ray showers (from the reaction $e^+e^- \rightarrow \gamma\gamma$) can be accurately located behind the separate segments of converters up to 4 radiation lengths in total thickness. Monte Carlo calculations indicate that this may be possible, but an experimental verification is desirable. It is not necessary to measure directions for the lower energy γ-rays from π^o decay (only the point of conversion is required) so that multiple converter designs are possible for such γ-rays. It may not be possible, however, to use individual converter thicknesses greater than about 1 radiation length if good efficiency for γ-rays with energy < 200 MeV is required. Monte Carlo calculations show that the conversion efficiency decreases rapidly with decreasing γ-ray energy below 200 MeV for converters of thickness 2 radiation lengths or more. To the extent that this is due to the re-absorption of secondaries, it will be necessary to use multiple converters, each of thickness close to 1 radiation length. (See Appendix I.)

Whatever converter design is developed for use with $e^+e^- \rightarrow \gamma\gamma$ and $e^+e^- \rightarrow \pi^o x$, it is important that its properties be verified in tagged γ-beams at both high and low energies. Total reliance on Monte Carlo shower calculations is unwise.

V Tagging

With our suggested detector (see Appendix I) we can sometimes tag both virtual photons of the process $e^+e^- \rightarrow (e^+e^-) + (\gamma^*\gamma^*) \rightarrow (e^+e^-) + X$. We will now try to give estimates, or at least plausibility arguments, for what one may expect in the detector from such processes. Our notation is shown in Fig. 11.

The Trigger requires two electromagnetic showers from charged particles with θ_1', $\theta_2' > 14$ mr plus detection of photons or charged hadrons. In order to discriminate against Bhabba scattering, the $e^\pm$ pair should be non-coplanar. A discussion of backgrounds is given by the tagging group[10]. The questions we will discuss are:

a) With what efficiency can we tag the virtual photons?

b) How often do we see tagged virtual photons and a hadronic system?

c) For what M_X range can we measure the invariant mass of the hadronic system?

d) What multiplicities do we expect?

e) What energies do we expect the particles to have?

f) What direction do we expect the particles to be going?

These questions are discussed in terms of the equivalent photon approximation.[11] The differential cross section for a particular reaction, $e^+e^- \rightarrow e^+e^-$ + something, is written:

$$d^4\sigma_{e^+e^-}/d\theta_1' d\theta_2' d\omega_1 d\omega_2 = \frac{N(\omega_1,\theta_1')\,N(\omega_2,\theta_2')}{\omega_1\,\omega_2}\, d\sigma_{\gamma\gamma} \qquad (5)$$

where $d\sigma_{\gamma\gamma}$ is the differential cross section for the corresponding two photon reaction, $\gamma\gamma \rightarrow$ something. For small θ_1', θ_2' the photons can be taken to be real.

Define $z = \omega/E$ and suppose θ_0 is the minimum electron angle for tagging a virtual photon. Then for $m_e/E \ll \theta_0 \ll 1$,

$$\eta(z,\theta_0) = \int_{\theta_0}^{\pi} N(\omega,\theta)\, d\theta = \frac{\alpha}{\pi}\left[(2-2z+z^2)\ln 2/\theta_0 + \frac{(2-z)^2}{4}\ln\left(\frac{z^2+\theta_0(1-z)}{(2-z)^2}\right)\right] \quad (6)$$

Equation 6 comes from Eqs. (3.1) and (A.7) of Reference 11. $\eta(z,\theta_0)$ is shown in Fig. 12 for $\theta_0 = 14$ mr. By comparing $\eta(z, 14\text{ mr})$ with $N(\omega) = \int_0^{\pi} N(\omega,\theta)\, d\theta$ as given in Reference 11, we see that at E = 15 GeV, 41% of the scattered leptons get outside 14 mr for $\omega = 7.5$ GeV; but this percentage drops to zero as ω drops to zero.

Now define $\lambda = M_x/2E$. From Eq. (5) we get

$$\left[\frac{E}{\sigma_{\gamma\gamma}(M_x)}\right]\frac{d\sigma_{e^+e^-}}{dM_x} = \frac{2}{\lambda}\int_0^{\ln(\frac{1}{\lambda})} dy\, \eta(\lambda e^{y},\theta_0)\,\eta(\lambda e^{-y},\theta_0) \quad (7)$$

where $\sigma_{\gamma\gamma}(M_x)$ = the cross section for $\gamma\gamma \to$ anything with mass M_x (we here make the approximation that $\sigma_{\gamma\gamma}$ is independent of the mass of the virtual photons). Above z = 0.1, $\eta(z, 14\text{ mr})$ is approximately independent of z. The integrand of Eq. (7) is then approximately constant over the entire range of integration provided $\lambda e^{-\ln(1/\lambda)} = \lambda^2 > 0.1$

For $\lambda > 0.3$ the Eq. (7) can be approximated by

$$\frac{E}{\sigma_{\gamma\gamma}(M_x)}\frac{d\sigma_{e^+e^-}}{dM_x} \approx 2.4\times 10^{-4}\,\frac{\ln(\frac{1}{\lambda})}{\lambda}$$

Below $\lambda = 0.3$ the integration must be done numerically. Fig. 12 shows $1/\sigma_{\gamma\gamma}(M_x) \frac{d\sigma_{e^+e^-}}{dM_x}$ for E = 15 GeV with both e^+ and e^- detected at angles greater than 14 mr.

Equations (6) and (7) are expressed in scale invariant form to permit easy extension to any energy. Such scale invariance doesn't hold for $\theta_0 \lesssim m_e/E$ because then m_e sets the scale.

Following Brodsky [12], who gives other references used in the estimation of $\sigma_{\gamma\gamma}$, we write $\sigma_{\gamma\gamma} \approx \sigma_0 + \sigma_1/M_x$. By factorization of the Pomeranchuk trajectory, $\sigma_0 = \frac{\sigma_T^{\infty}(\gamma N)}{\sigma_T^{\infty}(NN)} \gtrsim 0.24$ μb. σ_1 is estimated (from exchange degeneracy and Regge trajectories used to fit other processes) to be $\sigma_1 \approx 0.27$ μb GeV. For high M_x, $\sigma_{\gamma\gamma}(M_x)$ is nearly constant; so Fig. 13 portrays something proportional to the mass spectrum produced by the two photon process with double tagging above 14 mr. To get an idea of the event rates involved, note that with the above estimation for $\sigma_{\gamma\gamma}$, there should be about 3800 events detected between M_x = 9 and 12 GeV when the integrated luminosity is 10^{38}. (≈ 46 day run)

Figure 13 shows that the M_x distribution is high at low M_x even though the low ω used to produce the states are suppressed by the requirement of double tagging at finite angles. But we may not be able to use all of the tagged two-photon low M_x events. The M_x resolution of a double tagging system deteriorates at low Mx, for one of the photons then tends to have much lower energy than the other, and $\frac{\Delta M_x^2}{M_x^2} \approx \frac{\Delta E}{\omega}$ where ΔE = energy resolution of electromagnetic showers of energy E and ω = energy of the soft photon. For some purposes we will want to cut out those events for which ω is so low that we cannot get adequate $\frac{\Delta M_x^2}{M_x^2}$.

We begin to cut events when the minimum possible ω, $\omega_{min} = \frac{M_x^2}{4E}$, is ΔE, i.e., $\lambda = \frac{M_x}{2E} = \left(\frac{\Delta E}{E}\right)^{\frac{1}{2}}$. For NaI(Tl), $\Delta E/E \approx 0.02/E^{1/4}$(FWHM) at E = 15 GeV we begin to lose the ability to measure the mass of the hadronic system when $M_x \lesssim 2$.

We now ask ourselves what the events will look like. First we estimate the typical multiplicity, following reference 13. For a given M_x the charged multiplicity is expected on the basis of experience with hadrons, Mueller-Regge analysis, and the photon hadron analogy, to be of the form $\langle n \rangle = (.93 \pm .12)\ ln\ M_x^2 + \text{constant} + \theta\ (1/M_x)$.

Next, we consider the motion of the hadronic system. In Eq. 7, we made the change of variables $\omega_1 = \frac{M_x e^y}{2}$, $\omega_2 = \frac{M_x e^{-y}}{2}$. The momentum of the hadronic system is $P_x = \omega_1 - \omega_2 = M_x \sinh y$. Similarly the energy is $E_x = \omega_1 + \omega_2 = M_x \cosh y$ and the velocity is $P_x = \tanh y$. As in the derivation of Eq. 7, we have the average of $|\beta_x| = \langle|\beta_x|\rangle =$

$$\frac{\int_0^{\ln(1/\lambda)} dy \tanh(y)\, \eta(\lambda e^{y}, \theta_0)\, \eta(\lambda e^{-y}, \theta_0)}{\int_0^{\ln(1/\lambda)} dy\, \eta(\lambda e^{y}, \theta_0)\, \eta(\lambda e^{-y}, \theta_0)} \quad (8)$$

Similarly, $\langle E_x \rangle$, $\langle P_x \rangle$, etc., can be computed by replacing tanh(y) by $M_x \cosh y$, $M_x \sinh y$, etc. If λ is large enough so that $\eta(\lambda\, e^{\pm y}, \theta_0)$ is nearly constant, the integrals can be explicity evaluated.

$$\langle |\beta_x| \rangle = 1 - \frac{\ln(2/1-\lambda^2)}{\ln(1/\lambda)}$$

$$\langle E_x \rangle = M_x\ (1-\lambda^2)/2\lambda \ln(1/\lambda)$$

$$\langle |P_x| \rangle = M_x\ (1-\lambda)^2/2\lambda \ln(1/\lambda)$$

$$\langle E_x^2 \rangle = M_x^2/2 \left((1-\lambda^4)/2\lambda^2 \ln(1/\lambda) + 1 \right)$$

$$\langle P_x^2 \rangle = \langle E_x^2 \rangle - M_x^2$$

For $\lambda > 0.3$, $\langle |\beta_x| \rangle < 0.35$ and even for λ as low as 0.1 numerical evaluation of Eq. (8) gives $\langle |\beta_x| \rangle$ only 0.58. These numbers are to be compared with $\beta = 0.9$ for a 300 MeV/c pion.

If, for E = 15 GeV, we take the charge multiplicity for $M_x = 9$ GeV to be $\langle n \rangle = 0.93 \ln M_x^2 = 4.09$ and the neutral multiplicity to be 1/2 the charged multiplicity, the average energy per particle can be estimated to be about

$$\frac{\langle E_x \rangle}{3/2 \times 4.09} = 1.85 \text{ GeV} .$$

In the center of mass of the virtual photon pair, the perpendicular momentum component is expected to have the hadronic character $\frac{d\sigma}{dP_\perp^2} \propto e^{-7.6 P_\perp^2}$ ($p_\perp$ in GeV/c). For example, a pion with the typical lab energy of 1.85 GeV in a $M_x = 9$ GeV state and with a typical $P_\perp$ of 0.3 GeV/c will have an angle of 160 mr even if the virtual photons are at near zero angles. Thus the hadrons for the high M_x states are almost always going to get out of the beam pipe.

VI New Particles

As is pointed out by the New Particles Group [14] in this Summer Study, good electron and muon identification, combined with an overall energy measurement, is a powerful combination in searching for new particles, particularly heavy leptons. Excited leptons $e^*(\mu^*) \rightarrow e + \gamma$ $(\mu + \gamma)$ can be seen in a "neutral" detector by observing $e^+e^- \rightarrow e^+e^-$ $(\mu^+\mu^-) + \gamma$'s and then reconstructing an M^* distribution and looking for bumps in this distribution. Charged gauge and sequential leptons typically [14] have decays like $e' \rightarrow \nu_{e'}$ $e\,\bar{\nu}_e$ $(\nu_{e'}, \mu\,\bar{\nu}_\mu)$. The experimental signature in these cases is threefold: a) an acoplanar ee, $\mu\mu$, or $e\mu$ pair, b) the presence of hadrons as well as leptons, and c) the missing $P_\perp$ and E carried away by neutrinos.

Neutral heavy leptons, present in many gauge theories [14], have decays typically like $E^o \rightarrow e^+ \nu_e e^-(\mu^+ \nu_\mu e^-)$ or e^-+ hadrons, ν_e+ hadrons. In these cases, four leptons may be present in the final state. This characteristic combined with missing E and $P_\perp$ is a strong signature for their presence.

Given the excellent e, γ and μ identification properties of the neutral detector (such as that in Appendix I) and its good energy resolution, the above heavy lepton signatures should be detectable with high sensitivity.

VII ACKNOWLEDGEMENTS

The authors are grateful to L. H. O'Neill and R. L. Ford of the High Energy Physics Laboratory at Stanford for contributions to Section IV.

REFERENCES AND FOOTNOTES

1. J. Kadyk, PEP Summer Study Invited Paper.

2. G. Feldman and D. Hitlin: PEP Summer Study Contributed Paper, PEP-143.

3. Report on Weak Interactions, PEP Summer Study, PEP-157

4. D. Coyne, PEP Summer Study Invited Paper.

5. Engler et al., Nucl. Inst. Meth. 106, 189 (1973).

6. See discussion in Section V, Also See Fig. 11-12.

7. We assume NaI(Tl) Resolution Here. See PEP-155 for estimates for many Materials.

8. Barbiellini et al., Atti dell'Accademia Nazionale dei Lincei, 44, 233 (1968).

9. Berends et al., Nuclear Physics B68, 541 (1974) and Nuclear Physics B57, 381 (1973).

10. Report on $\gamma\gamma$ Tagging, PEP Summer Study, PEP-175.

11. Brodsky, Kinoshita, Terazawa, Phys. Rev. D4, 1532 (1971).

12. S. Brodsky, Journal de Physique 35, C2-62 (1974).

13. Chen, SLAC-PUB-1434 (1974), submitted to Phys. Rev.

14. Report on New Particles, PEP Summer Study, PEP-174.

15. These rates assume the working luminosity given by B. Richter: PEP Summer Study Contributed Paper, PEP-140.

TABLE 1

Models for Hadron Production at PEP
$s = 900\ GeV^2$

	MODEL I "hard π"	MODEL II "soft π"
Average π energy (GeV)	2.20	0.57
Average total multiplicity	13.6	52.6
$\sigma_{TOT}(e^+e^- \rightarrow \text{hadrons})$	$4.5 \times 10^{-34} cm^2$	$1.6 \times 10^{-32} cm^2$
Events/(1 hour = $10^{35} cm^{-2}$)	45	1600
$R = \sigma_{TOT}/_{\mu\mu}$	5	179
π^o's produced/(1 hour = $10^{35} cm^{-2}$)	204	28200

All rates assume the working luminosity specified in Reference 15.

TABLE 2

Corrections to σ_{TOT}

Effect	Correction	Error	
fewer than 2 charged	+ 5% or less	± 1%	some model dependence
$E_{TOT} < 15$ GeV	+ 8% or less	± 2%	some model dependence
beam-gas	- 5% or less	± 1%	very straightforward
ee → ee, μμ	large	± 1%	very straightforward
ee → ee hadrons	large?	± 5%	requires lots of work with data, but E_{tot} helps (see Fig. 4).

FIGURE CAPTIONS

1. The integral cross section for π^o production as a function of P_o at PEP according to Models I and II. $(\sigma(cm^2) = \int_{P_o}^{\infty} dP_{\pi^o} (d\sigma/dP_{\pi^o}))$.

2. The integral cross sections for γ production as a function of P_o at PEP according to Models I and II.

3. E_{TOT}^{est} distributions obtained from the energy algorithm discussed in Section II.

4. The estimated experimental M_x distributions from $e^+e^- \rightarrow$ hadrons, and $\gamma\gamma \rightarrow$ hadrons. Leptons in $\gamma\gamma$ final states are removed.

5. The decay photon energy spectra according to Models I and II. Plotted is photons/(0.1 GeV) vs E (GeV).

6. The two photon mass squared distributions for all photon pairs, as obtained for NaI(Tl) using the Monte Carlo described in Section III.

7. Mass squared plot showing no background separation between π^o and η^o, as obtained for NaI(Tl) using the Monte Carlo of Section III.

8. π^o identification efficiency versus E_π, using the Model I energy spectrum, as a functional of number of background γ's. Results are shown for NaI(Tl) and Pb glass. Monte Carlo of Section III generated curves.

9. π^o identification efficiency versus number of π^o's produced, as calculated from Monte Carlo of Section III using the energy spectrum of Model I, and Model II. Results are shown for NaI(Tl) and Pb glass.

10. π^o identification efficiency versus number of background photons, generated using a background spectrum $dn/dE \sim \exp(-E/0.1)$, E in GeV.

11. Definition of notation for the process $e^+e^- \rightarrow e^+e^-$ + hadrons.

12. The function $\eta(z,\theta_o)$ defined in equation (6), for $\theta_o = 14$ mr.

13. The quantity $(d\sigma/dM_x)\,\sigma_{\gamma\gamma}(M_x)$ versus $\lambda = M_x/E_o$. The cutoff due to NaI(Tℓ) resolution is shown. Integrated $L = 10^{38}\,cm^{-2}$ represents approximately a 46 day run at PEP[15].

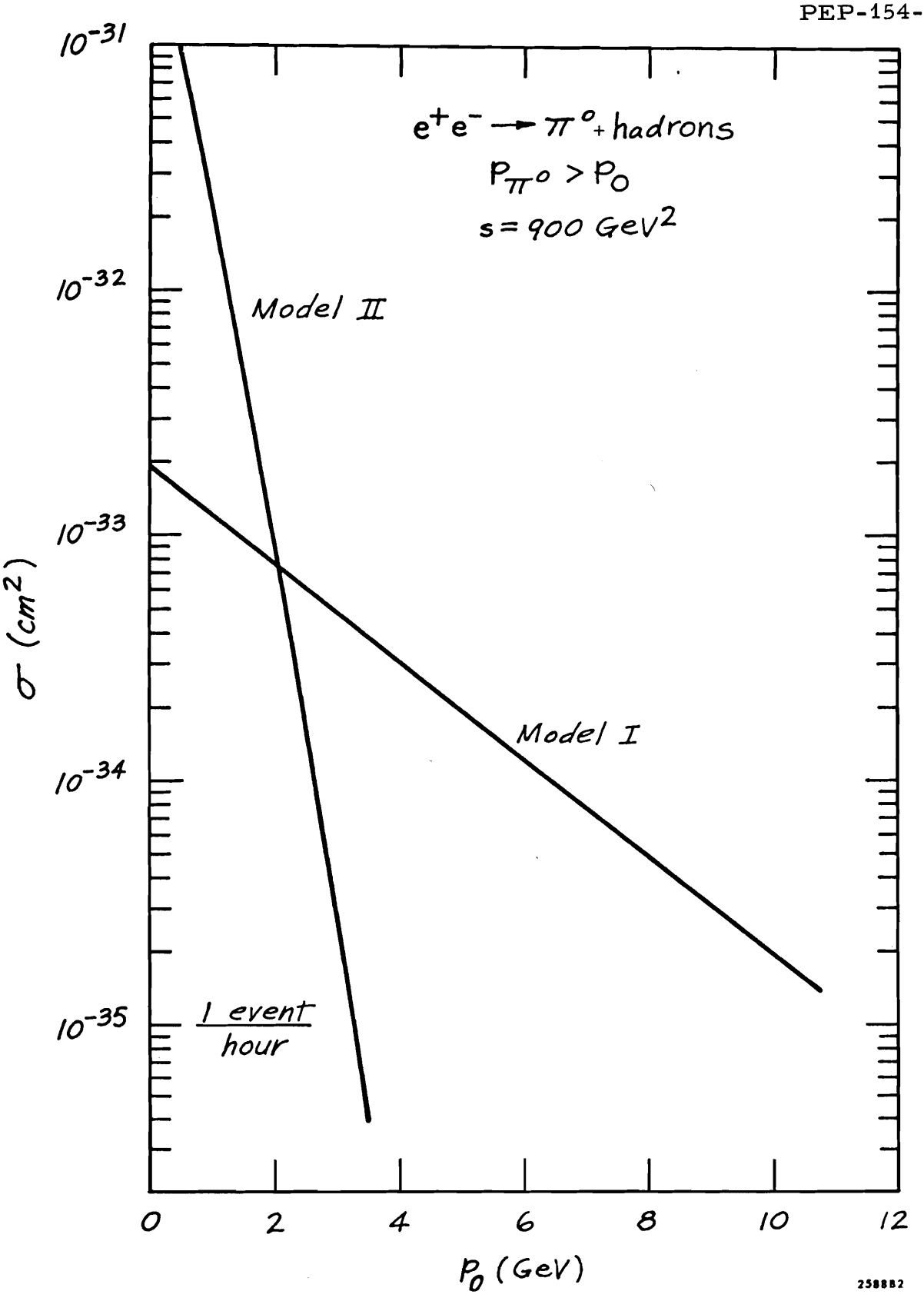
$e^+e^- \rightarrow \pi^o$ + hadrons
$P_{\pi^o} > P_0$
$s = 900\ GeV^2$
Model II
Model I
1 event / hour
10^{-31}
10^{-32}
10^{-33}
10^{-34}
10^{-35}
$\sigma\ (cm^2)$
0
2
4
6
8
10
12
P_0 (GeV)
258882

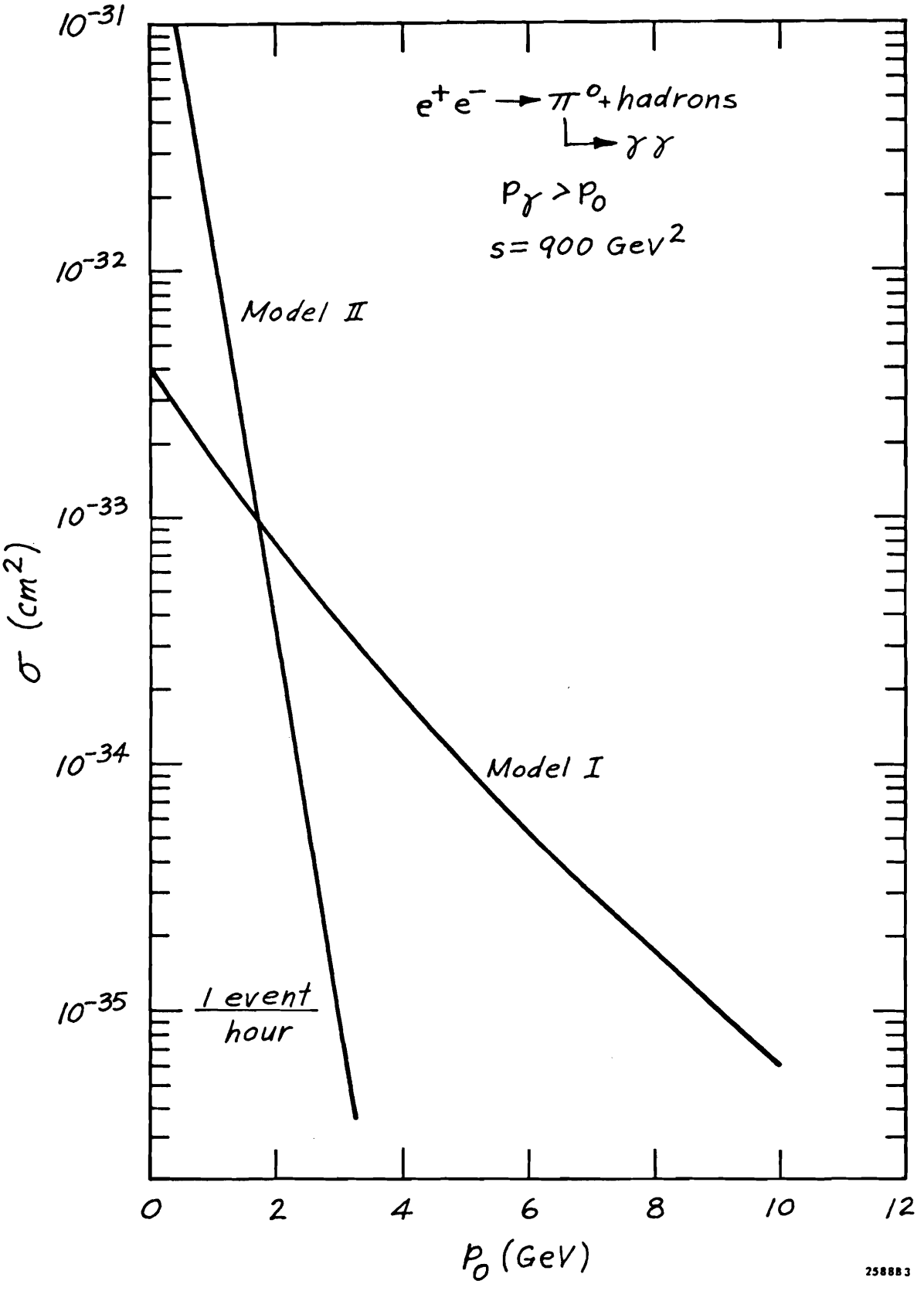
10^{-31}
10^{-32}
10^{-33}
10^{-34}
10^{-35}
σ (cm^2)
$e^+e^- \rightarrow \pi^0$ + hadrons
$\hookrightarrow \gamma\gamma$
$p_\gamma > p_0$
$s = 900$ GeV^2
Model II
Model I
1 event / hour
0
2
4
6
8
10
12
p_0 (GeV)
258883

Fig. 2

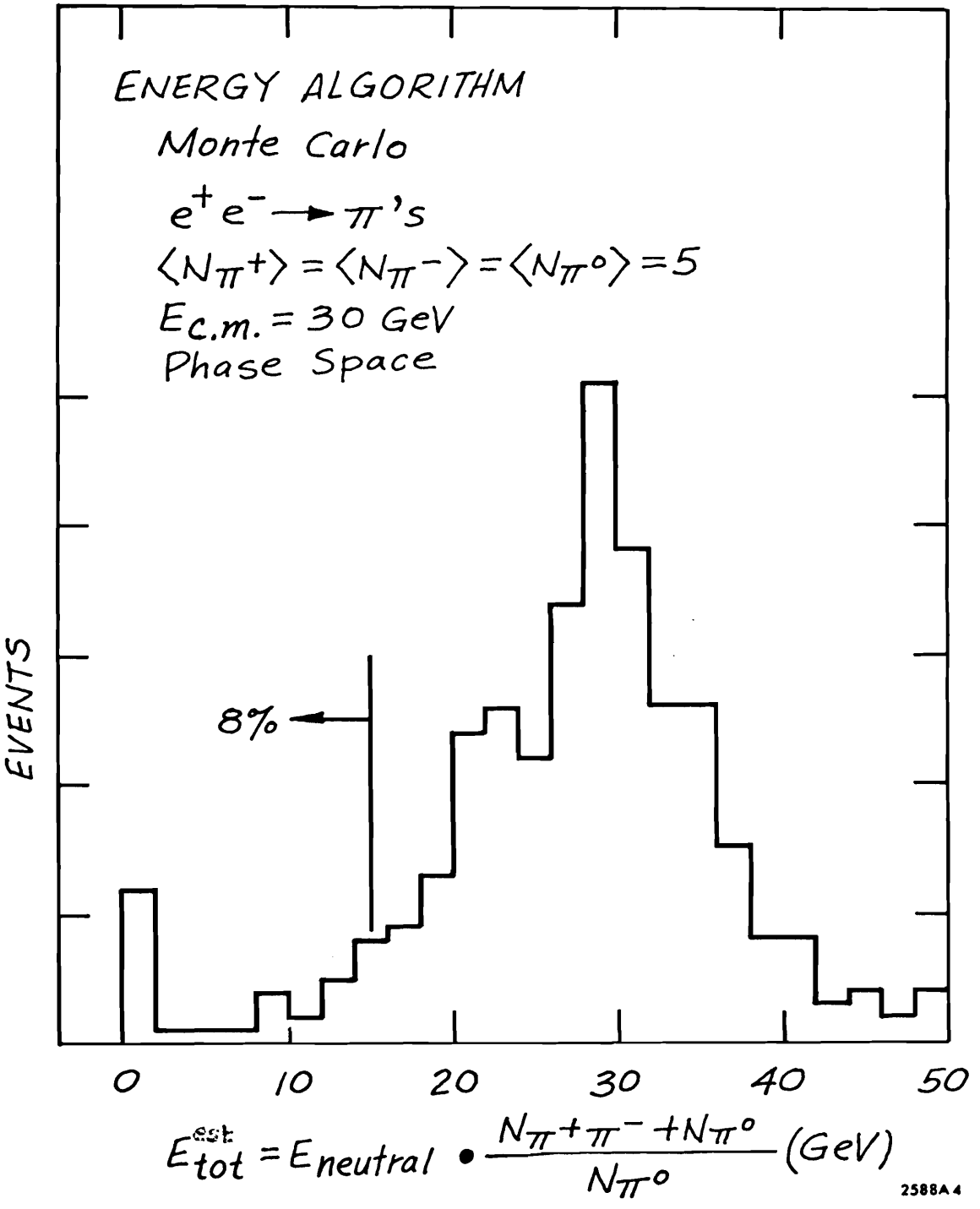
ENERGY ALGORITHM
Monte Carlo
$e^+e^- \rightarrow \pi$'s
$\langle N_{\pi^+} \rangle = \langle N_{\pi^-} \rangle = \langle N_{\pi^0} \rangle = 5$
$E_{c.m.} = 30$ GeV
Phase Space
8%
EVENTS
0
10
20
30
40
50
$E_{tot}^{est} = E_{neutral} \cdot \frac{N_{\pi^+\pi^-} + N_{\pi^0}}{N_{\pi^0}}$ (GeV)
2588A4

Fig. 3

Approximate inclusive spectrum $e^+e^- \rightarrow$ hadrons, total hadron energy "trigger", $d\sigma/dMx$ vs. λ, lepton in final state are $\sim$ subtracted. Assuming "hard π" model, $\langle N_{\pi^+} \rangle = \langle N_{\pi^-} \rangle = \langle N_{\pi^0} \rangle$, hadron calorimeter resolution $\simeq \pm 30\%$, $\sigma_{\gamma\gamma}(Mx) = 0.3$ nb, $E_0 = 15$ GeV.

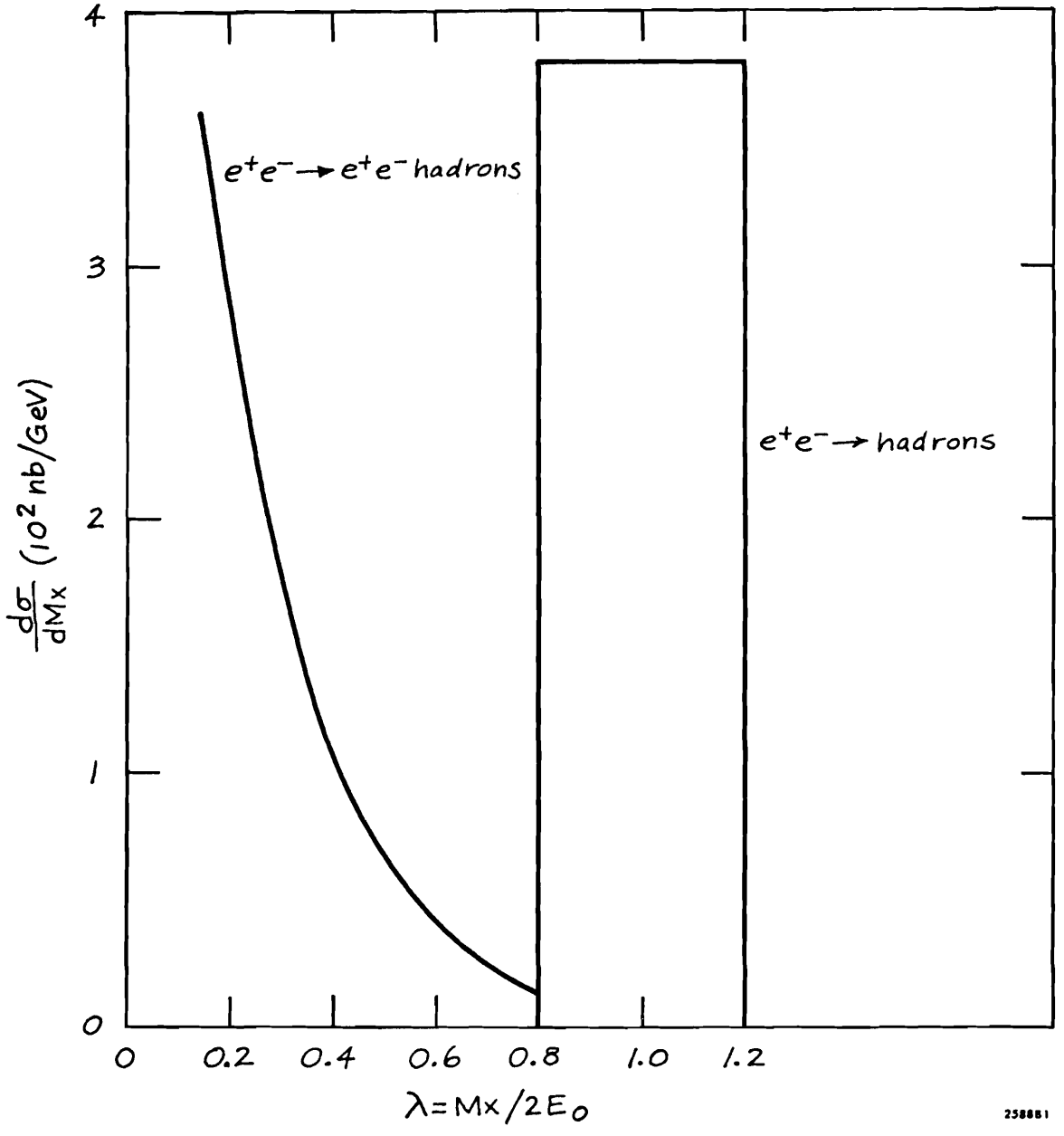

Fig. 4

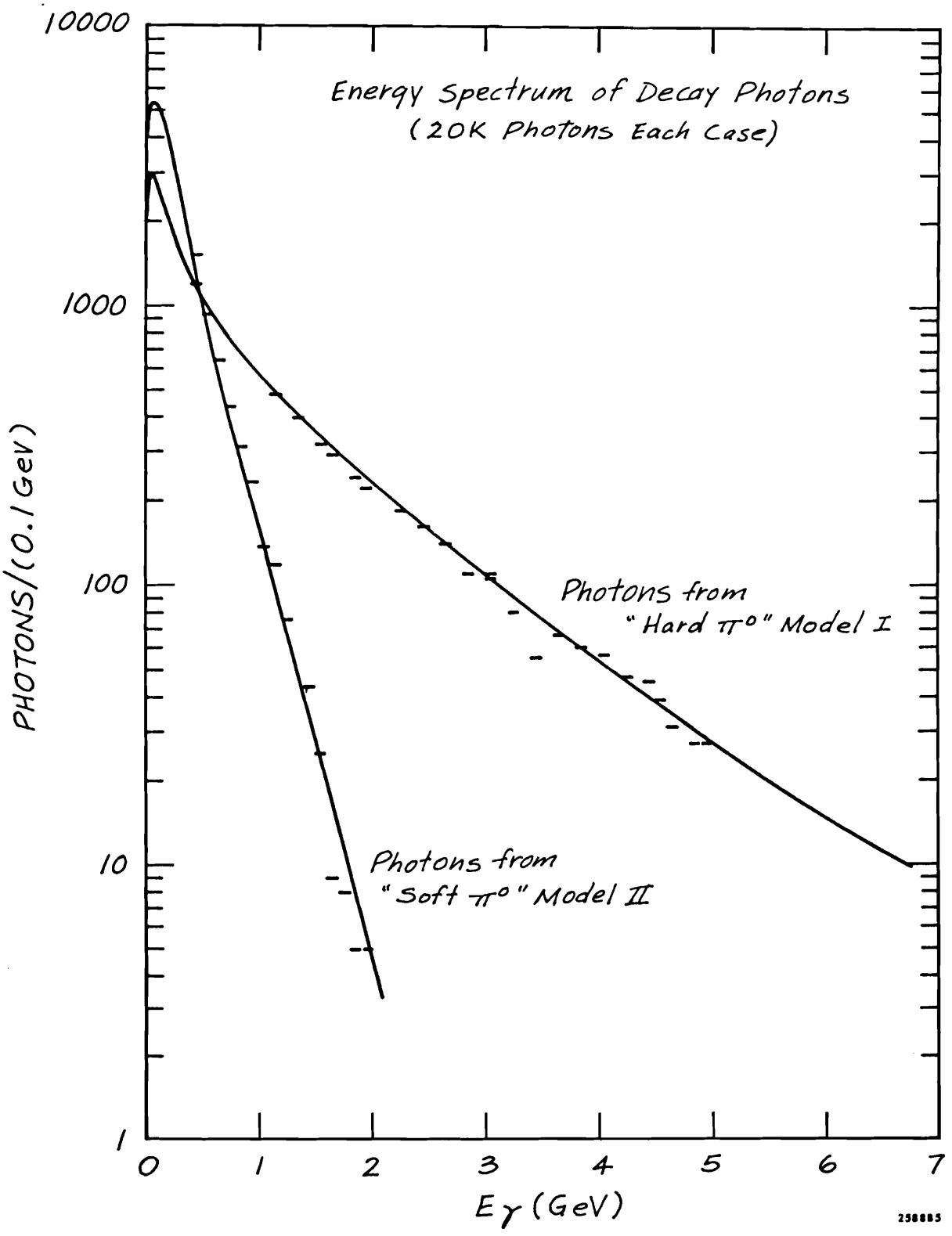
Energy Spectrum of Decay Photons
(20K Photons Each Case)
Photons from
"Hard π°" Model I
Photons from
"Soft π°" Model II
PHOTONS/(0.1 GeV)
Eγ (GeV)
10000
1000
100
10
1
0
1
2
3
4
5
6
7
258885

Fig. 5

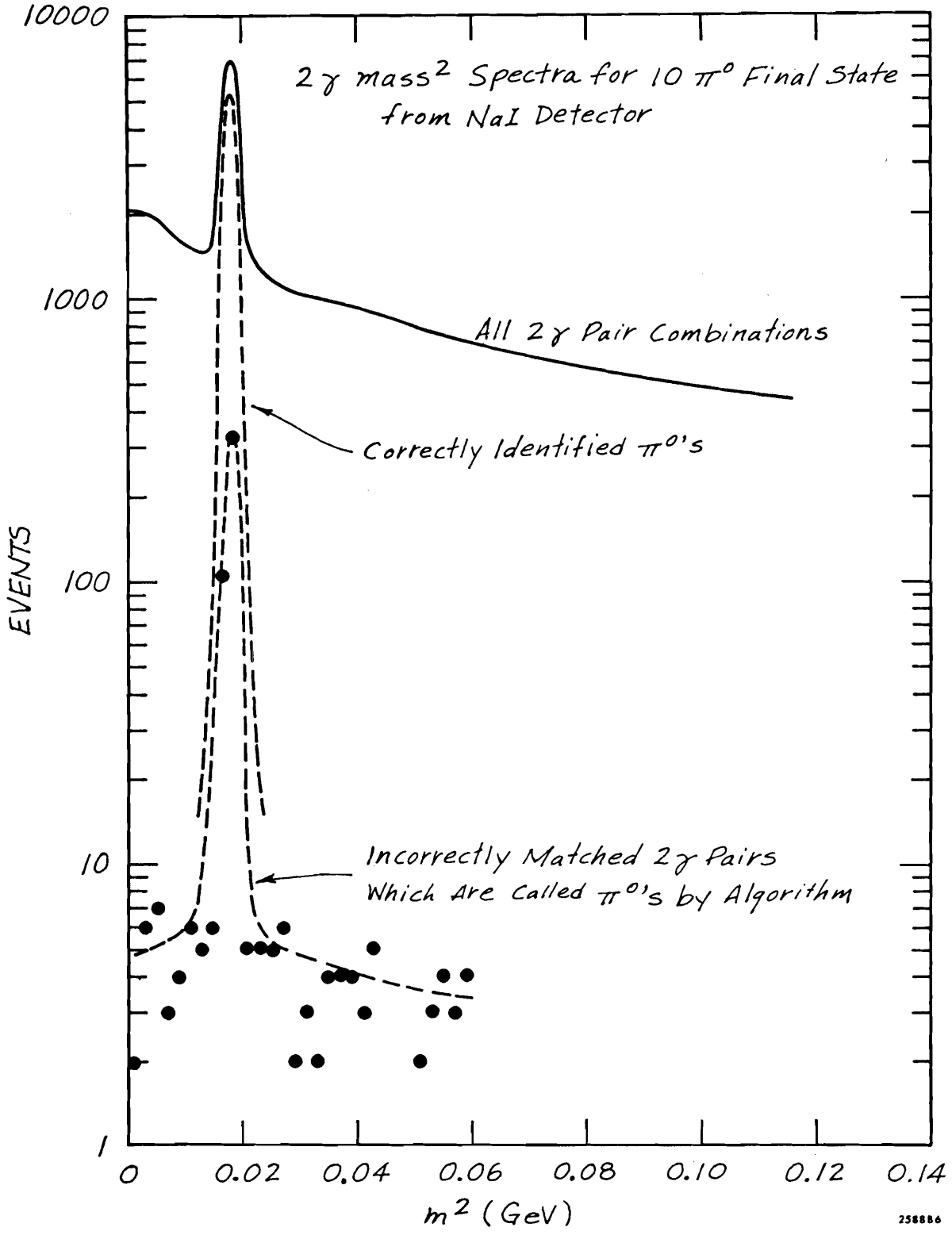
10000
1000
100
10
1
EVENTS
2γ mass² Spectra for 10 π⁰ Final State
from NaI Detector
All 2γ Pair Combinations
Correctly Identified π⁰'s
Incorrectly Matched 2γ Pairs
Which Are Called π⁰'s by Algorithm
0
0.02
0.04
0.06
0.08
0.10
0.12
0.14
m² (GeV)
258886

Fig. 6

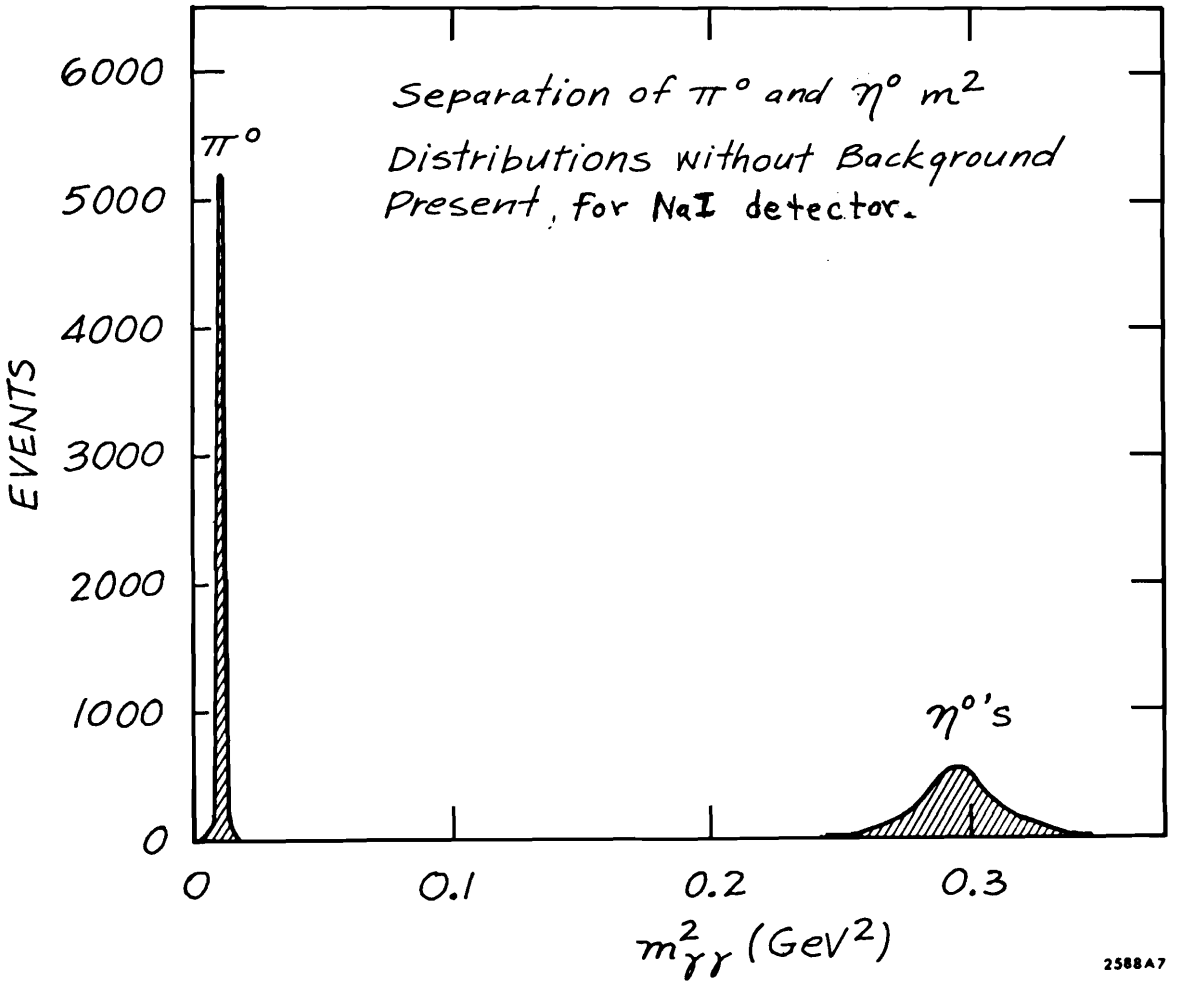
Separation of π^0 and η^0 m^2
Distributions without Background
Present, for NaI detector.
π^0
η^0's
EVENTS
6000
5000
4000
3000
2000
1000
0
0
0.1
0.2
0.3
$m^2_{\gamma\gamma}$ (GeV^2)
2588A7

Fig. 7

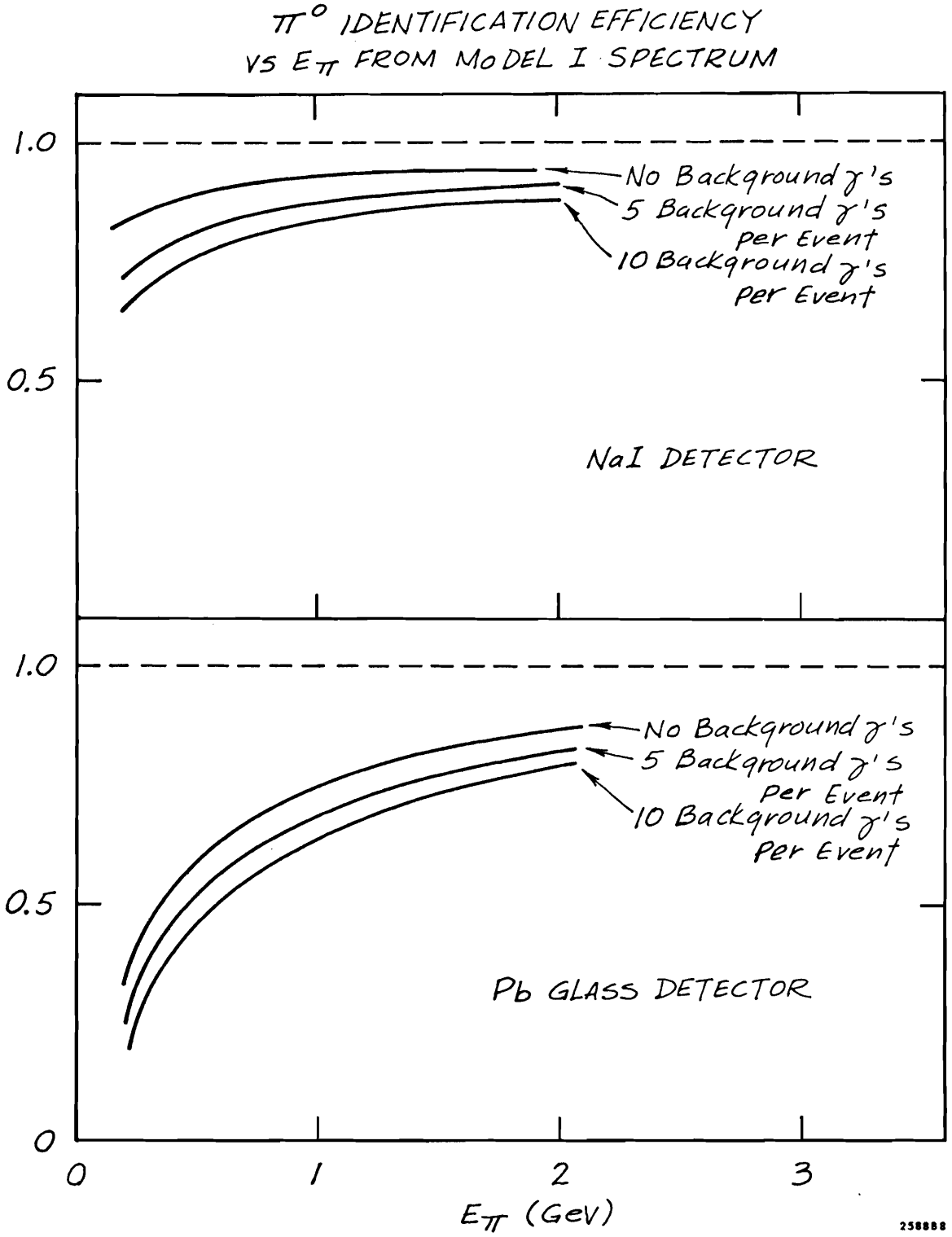
π^0 IDENTIFICATION EFFICIENCY
VS E_π FROM MODEL I SPECTRUM
1.0
0.5
No Background γ's
5 Background γ's per Event
10 Background γ's per Event
NaI DETECTOR
1.0
0.5
0
No Background γ's
5 Background γ's per Event
10 Background γ's per Event
Pb GLASS DETECTOR
0
1
2
3
E_π (GeV)
258888

Fig. 8

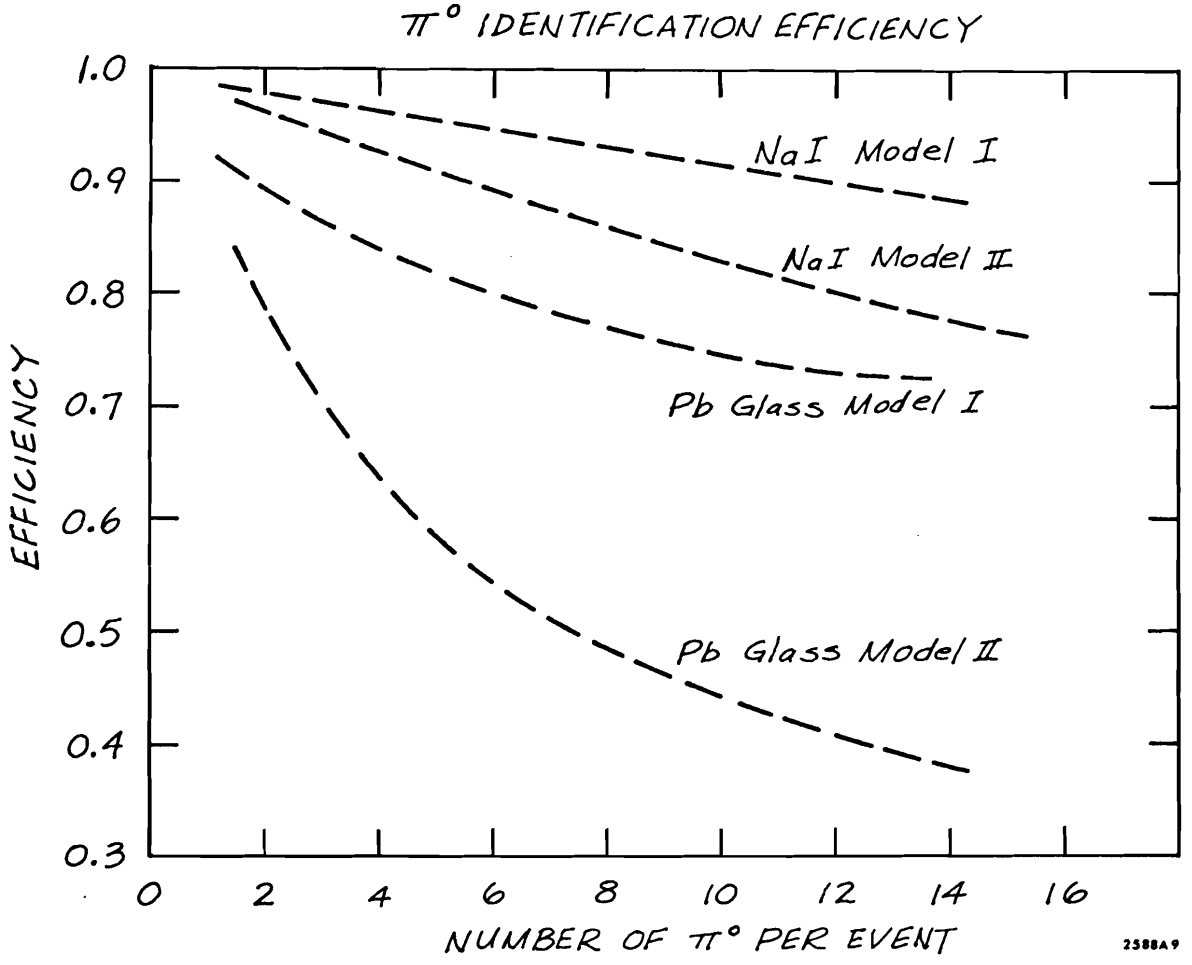
π° IDENTIFICATION EFFICIENCY
1.0
0.9
0.8
0.7
0.6
0.5
0.4
0.3
EFFICIENCY
NaI Model I
NaI Model II
Pb Glass Model I
Pb Glass Model II
0
2
4
6
8
10
12
14
16
NUMBER OF π° PER EVENT
2588A9

Fig. 9

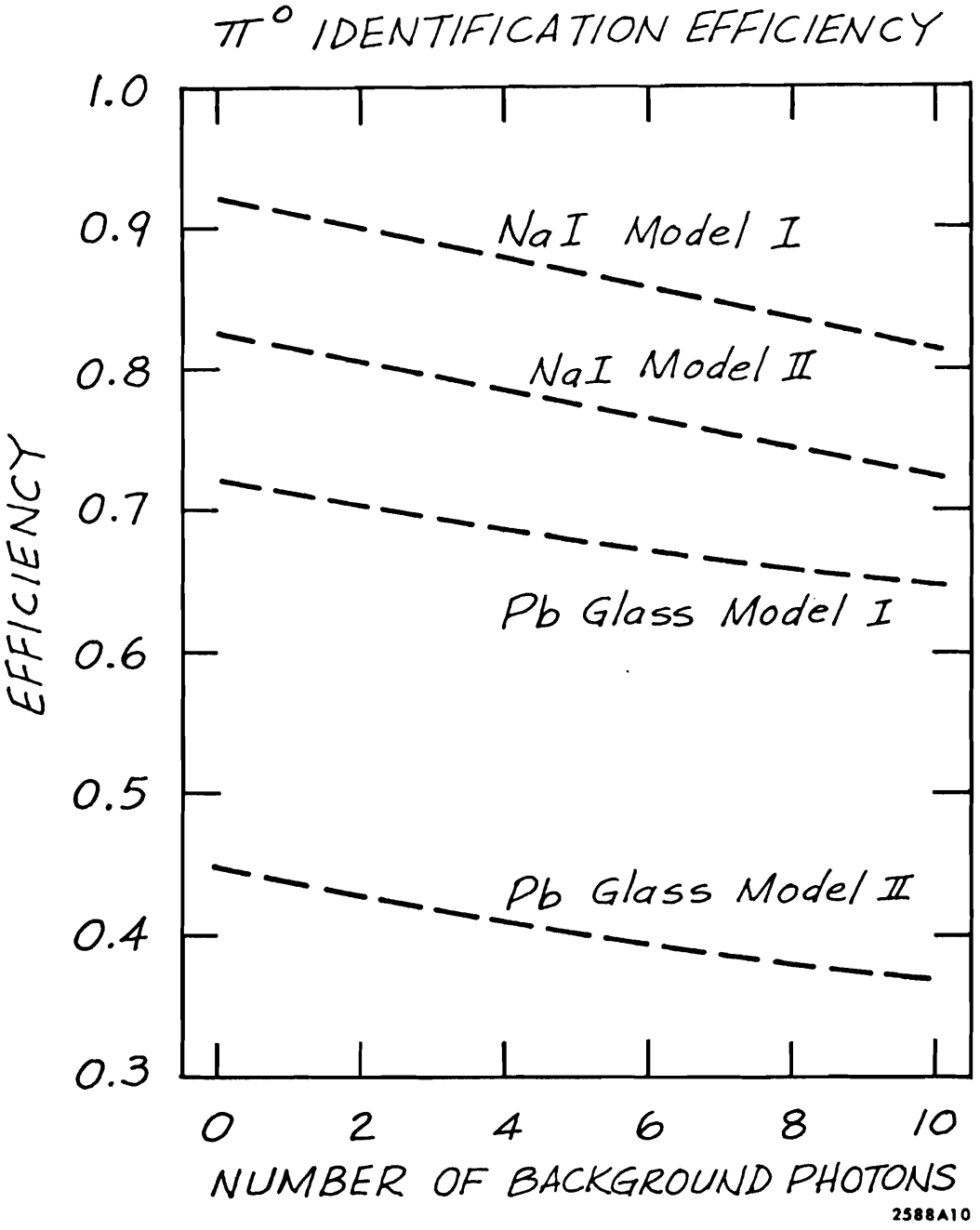
π° IDENTIFICATION EFFICIENCY
1.0
0.9
0.8
0.7
0.6
0.5
0.4
0.3
EFFICIENCY
NaI Model I
NaI Model II
Pb Glass Model I
Pb Glass Model II
0
2
4
6
8
10
NUMBER OF BACKGROUND PHOTONS
2588A10

Fig.10

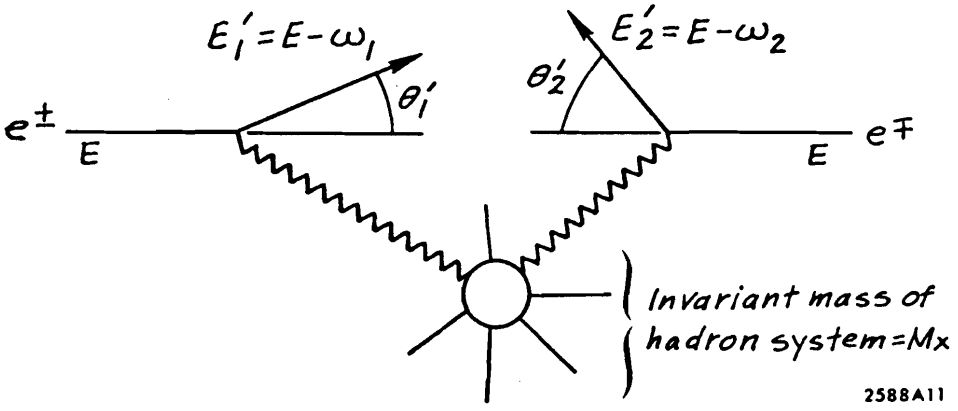
$E_1' = E - \omega_1$
θ_1'
$E_2' = E - \omega_2$
θ_2'
$e^{\pm}$
E
E
$e^{\mp}$
Invariant mass of
hadron system = Mx
2588A11

Fig. 11

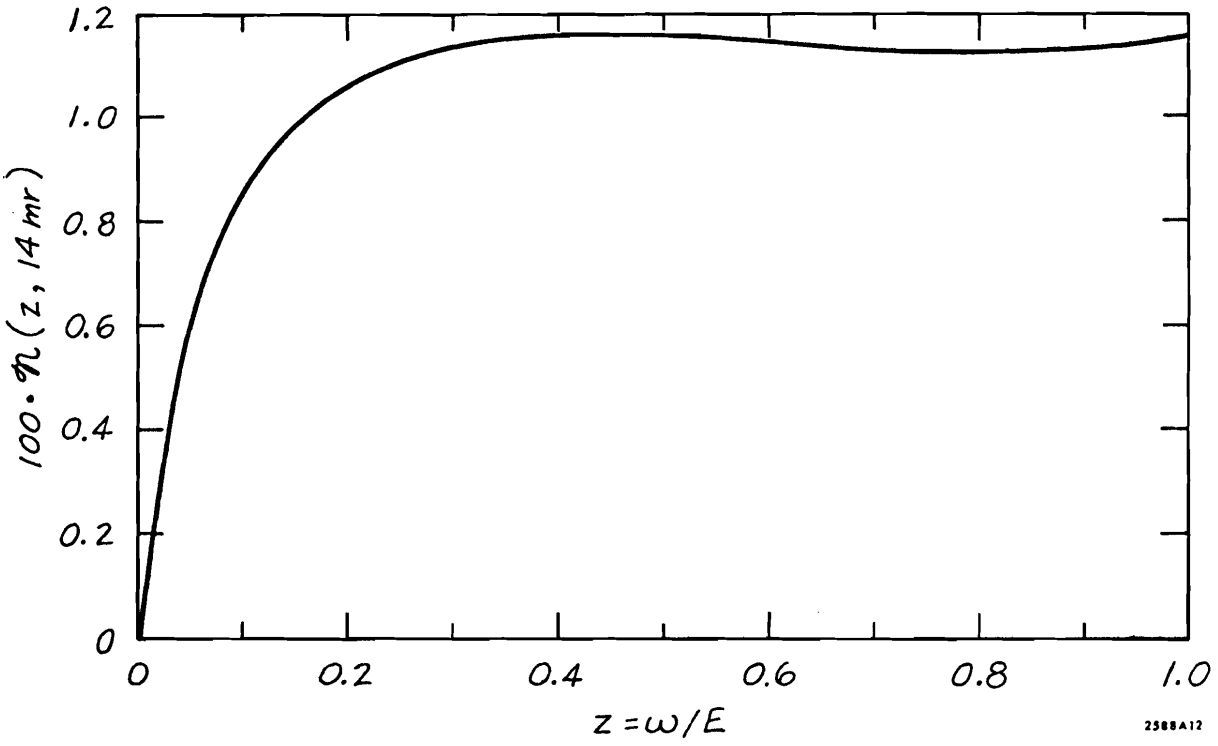

Fig. 12

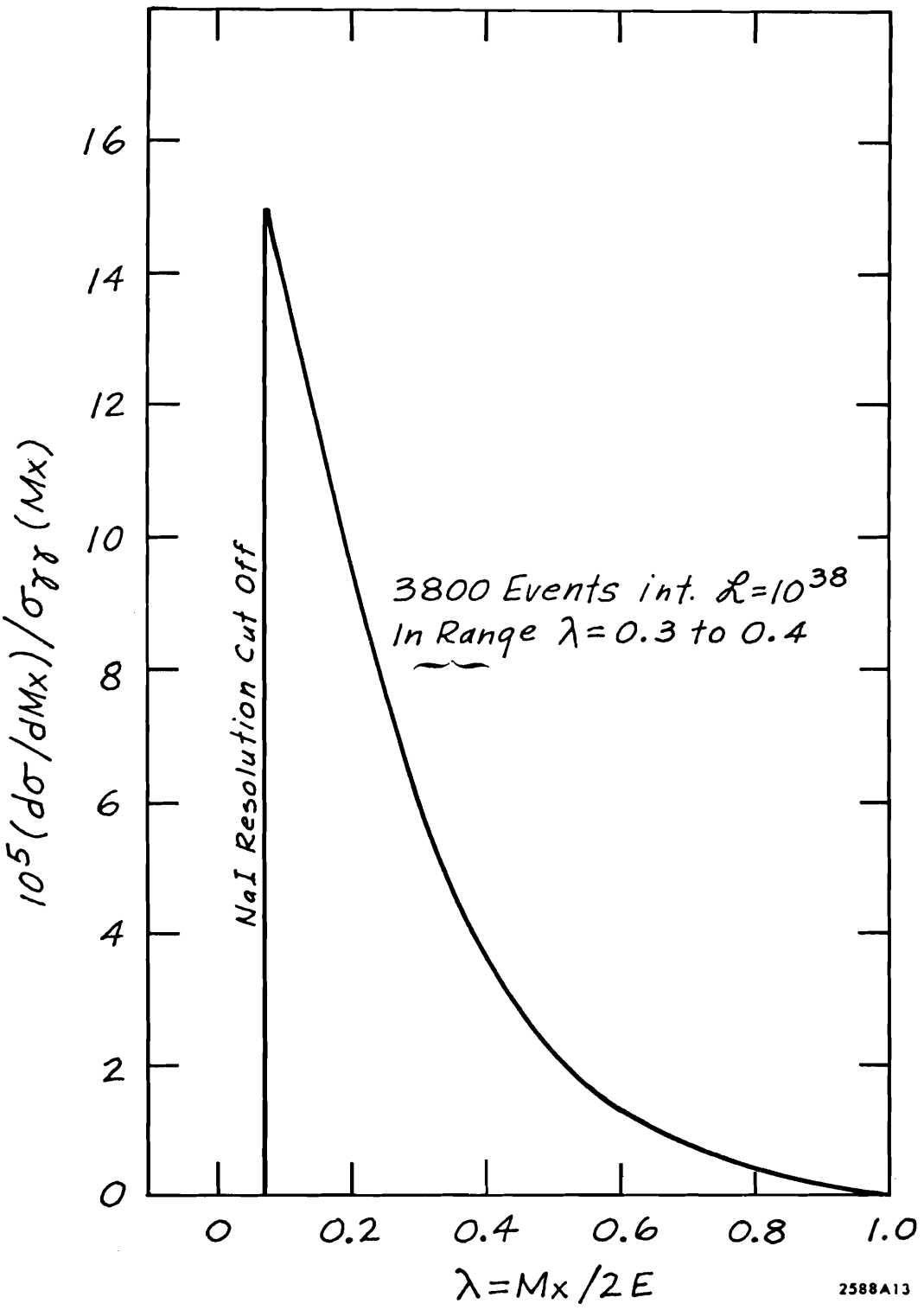
16
14
12
10
8
6
4
2
0
0
0.2
0.4
0.6
0.8
1.0
$10^5(d\sigma/dMx)/\sigma_{\gamma\gamma}(Mx)$
$\lambda = Mx/2E$
NaI Resolution Cut Off
3800 Events int. $\mathcal{L}=10^{38}$
In Range $\lambda = 0.3$ to 0.4
2588A13

Fig. 13

APPENDIX I: A NEUTRAL DETECTOR DESIGN

I. Description of the "Neutral" Detector.

The whole detector consists of 4 parts:

A. Central neutral detector;

B. Calorimeter with magnetized iron; and

C. Calorimeter with the same structure as in B but with umagnetized iron.

D. Luminosity monitor, and $\gamma\gamma$ tagging device.

The following is a brief description of each part. Figs. 1 and 2 show cross sections of the detector $\perp$ and $\parallel$ to the beam.

A. The Central Neutral Detector.

The main purpose of this part is to make a precise measurement of γ's, both in energy and direction, over a solid angle of 4π. In addition it makes possible the measurement of charge particle directions over a 4π solid angle, which also reveals the interaction vertex.

The guide lines for the geometrical design of this part are:

1. 4π solid angle;
2. minimum volume;
3. available space for photomultipliers;
4. exit space for cables; and
5. reasonably quick access.

It consists of 3 sections; a stationary central section and two end sections which can be moved on rails along the beam direction (see schematic in Fig. 4).

The central section is roughly a cylindrical volume with the beam as an axis of symmetry. The internal and external radii are $\approx$ 12 cms and 80 cms, respectively, and the length is $\approx$ 60 cms.

Each of the end sections consists of two semicircular discs with their planes tilted at about 15^{o} to the vertical. This tilt helps satisfy requirements 3 and 4 above. Fig. 3 shows a possible layout of the end section.

The maximum length of the whole central detector along the beam is 200 cms, and the maximum radius at any point of its cylindrically symmetric profile is $\approx$ 100 cms.

In each section, a particle from the interaction region passes in sequence through the following:

1. 1/4" scintillation counter divided azimuthally into 8 parts;
2. 6 planes of wire chambers covering a distance of $\approx$ 15 cms;
3. 1/4" scintillation counter also divided azimuthally into 8 parts in one to one correspondence with (1). Hence, coincidence requirement for the straight charged particles, if desired, is very simple;
4. a radiator - position finder stage made of $4 \times \frac{1}{2}$" r.ℓ (NaI), followed by 2×1 r.ℓ (NaI). These radiators are separated by wire planes. The radiators and wire planes are distributed along a distance of $\approx$ 30 cms. This stage is flexible and could be somewhat changed to optimize its performance; and
5. a thick absorber of $\approx$ 10 r.ℓ of NaI making the total absorber including the radiator = 14 r.ℓ.

The thick absorber is divided into square sections $\approx$ 14 cms on the side. Using a 5" photomultiplier tube, $\approx 2/3$ of the light emerging from the square end is collected. These sections also serve as a

coarse digitizer for the γ direction with angular accuracy $\approx \pm 7$ cms at a distance of 80 cms from the interaction region, ie $\pm 5^{o}$.

The above geometrical design is by no means rigid. Some variations in shape and dimensions along the same general guide lines can be made to optimize its performance.

B. Magnetized Iron Calorimeter.

This part has an octagonal cross section $\perp$ to the beam. The radial thickness, ≈ 90 cms, is composed of 60 cm of iron and 24 cms of liquid scintillator, with cylindrical wire planes at the entrance and exit. The maximum length along the beam is ≈ 4.4 meters. The angular range of this section is $\Delta\phi=2\pi$, $40^{o} < \theta < 140^{o}$.

The iron is divided into 7 sections, 5, 5, 10, 10, 10, 10, and 10 cms thick sandwiched with 6 x 4 cms of liquid scintillator.

A coil is wound at each vertex of the octagon (see Fig. 1). Hence, the magnetic field is circular around the beam direction. Each coil requires $\approx$ 100 amps at 150 volts to produce a field of 18 k.g in the iron.

The momentum resolution of this part is dominated by multiple scattering. Δ p/p for a 15 GeV $\mu \approx 20\%$.

Because the iron filter is not sufficiently thick, a good separation of π's and μ's requires the measurement of the spatial distribution of hadron showers. This can be done by adding some wire chambers inside the iron layers or by replacing the liquid scintillator by layers of proportional liquid tubes.

C. Non-Magnetic Plugs.

The construction of these plugs is identical to part B except that the magnetic field is absent. They need no additional description, except to say that they complete a 4π solid angle for the calorimeter.

D. Luminosity Monitor, and $\gamma\gamma$ Tagging Device.

Provision is made for the operation of a $\gamma\gamma$ tagging device in the angular region 14-131 mr seen by the main detector. This device will be designed to serve as a luminosity monitor also. Its construction is compatible with a free length of ± 5 meters about the interaction region. This device is not shown in Figures 1 and 2.

2. GENERAL SPECIFICATIONS FOR INTERACTION REGION AND DETECTOR AND COST ESTIMATES:

I. Dimensions needed for apparatus rooms

- A. Prime apparatus - 10 cu. meters
- B. Appendages - 60 cu. meters
- C. Close electronics distance - 40 meters
- D. Distant electronics distance - 40 meters (monitoring)
- E. Support equipment
  1. Gas
  2. General electronics
  3. Magnet power

II. Interaction Region

- A. Free length required is $\pm$ 5 meters.

III. "Cable" requirements.

- A. Counter and wire chambers - 1200 signal cables, 1200 H.V. cables
- B. Gas lines
- C. Monitor lines

} Yes - (5" diameter gas pipe)

IV. Loading and Moving

- A. Weight - 300 tons
- B. Move - in/out scheme (i.e., no quick-change area needed)
- C. Cranes needed - 50 ton capacity
- D. Crane coverage needed - 10 x 6 meters

V. Safety and Access

A. Radiation walls needed for on-line access - one

B. Dangerous gases/liquids (ventilation needed) - maybe

C. Air conditioning/dehumidification needed for chamber survival - no

VI. Luminosity Monitor

A. Do you need your own - yes

VII. Tagging system

A. Do you need your own for background subtraction - yes

VIII. Shielding apparatus, how much and where

A. We would like the shielded counting house to be about 40 meters away from interaction region.

SUMMARY COST INFORMATION

CENTRAL NEUTRAL DETECTOR		$
NaI	2060 Liters	900 K
Scint	60 sq. ft., 1/4" at $50/sq. ft.	3 K
5" PMT's & Bases	470	125 K
Spark Chambers		40 K
Power Supplies	3kW	25 K

MAGNETIC CALORIMETER		$
Iron	200 tons at .5K/ton	100 K
Liq. Scint.	1500 Liters at 1/lit.	1.5 K
PMT's and Bases	300	70 K
Sp. Chmbs		160 K
Magnet Power 200 kW.		

PLUG CALORIMETER		
Iron	60 tons	30 K
Liquid Scint	300 Liters	.3 K
PMT's and Bases	60	14 K
Spark Chmbs		30 K

GENERAL		
Signal Cables	1200	
H.V. Cables	1200	

TOTAL ≈ $1.5 Million

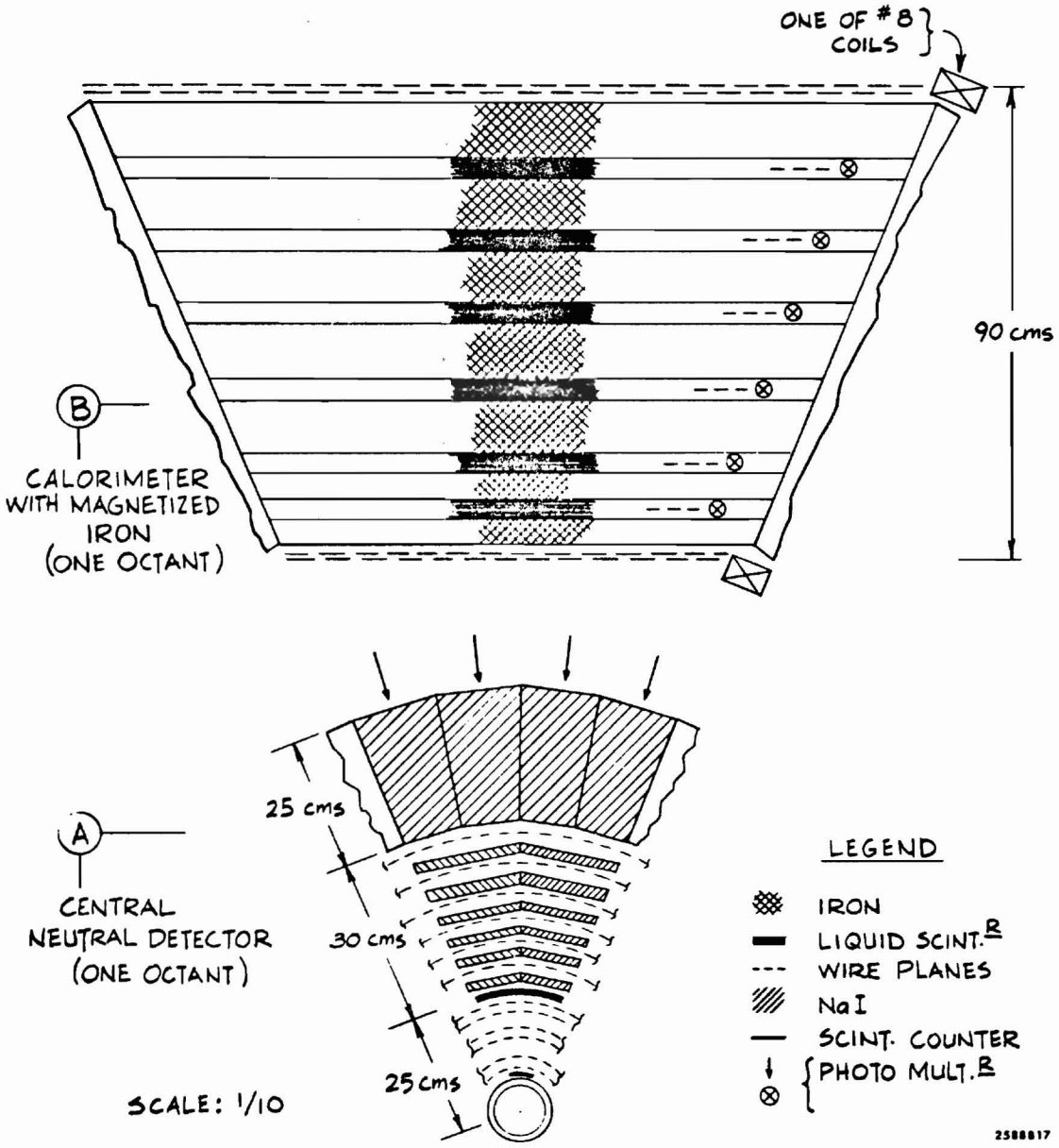

Fig. I-1

A section through the detector transverse to the beam.

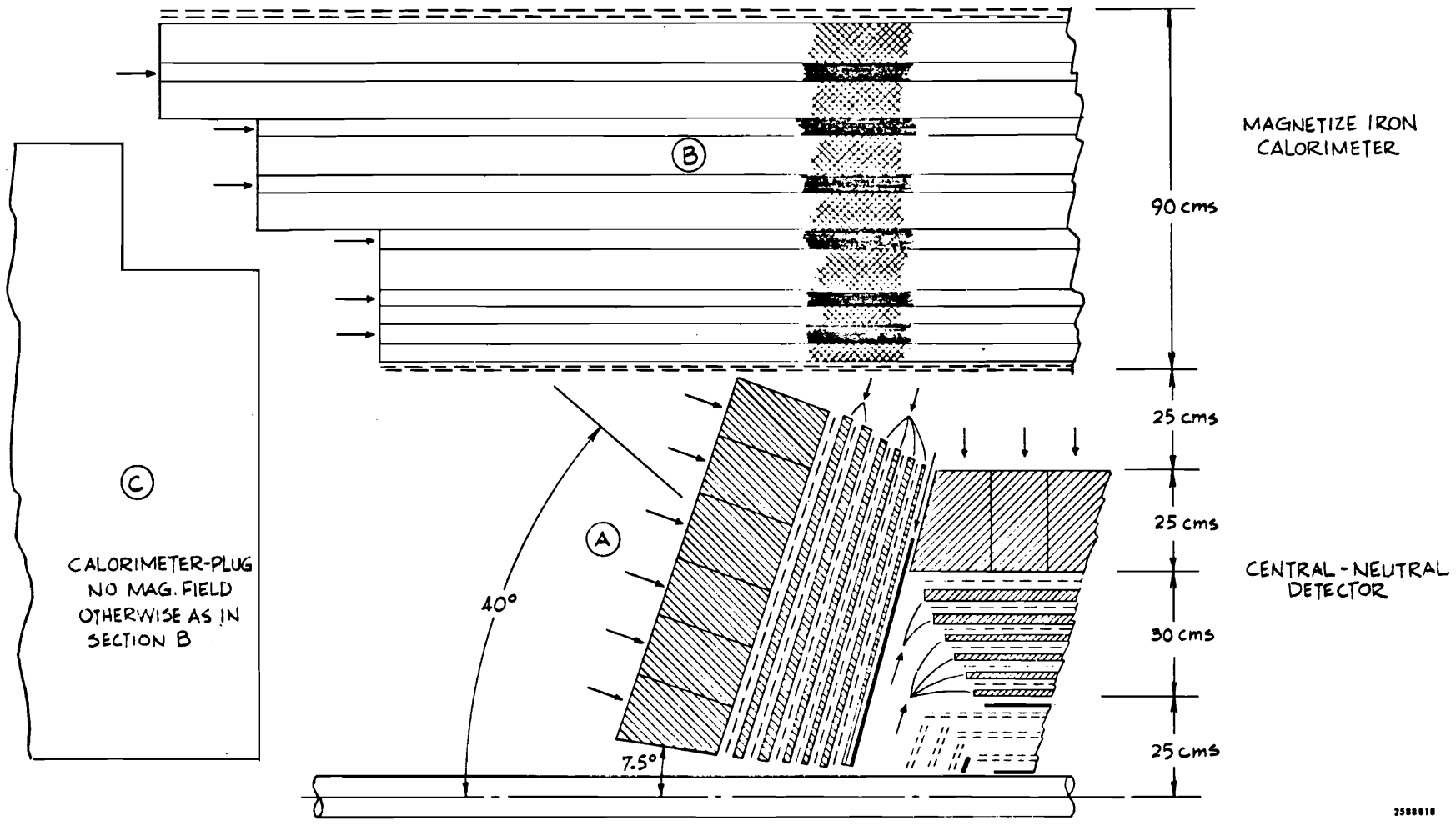

Fig. I-2

A section through the detector parallel to the beam.

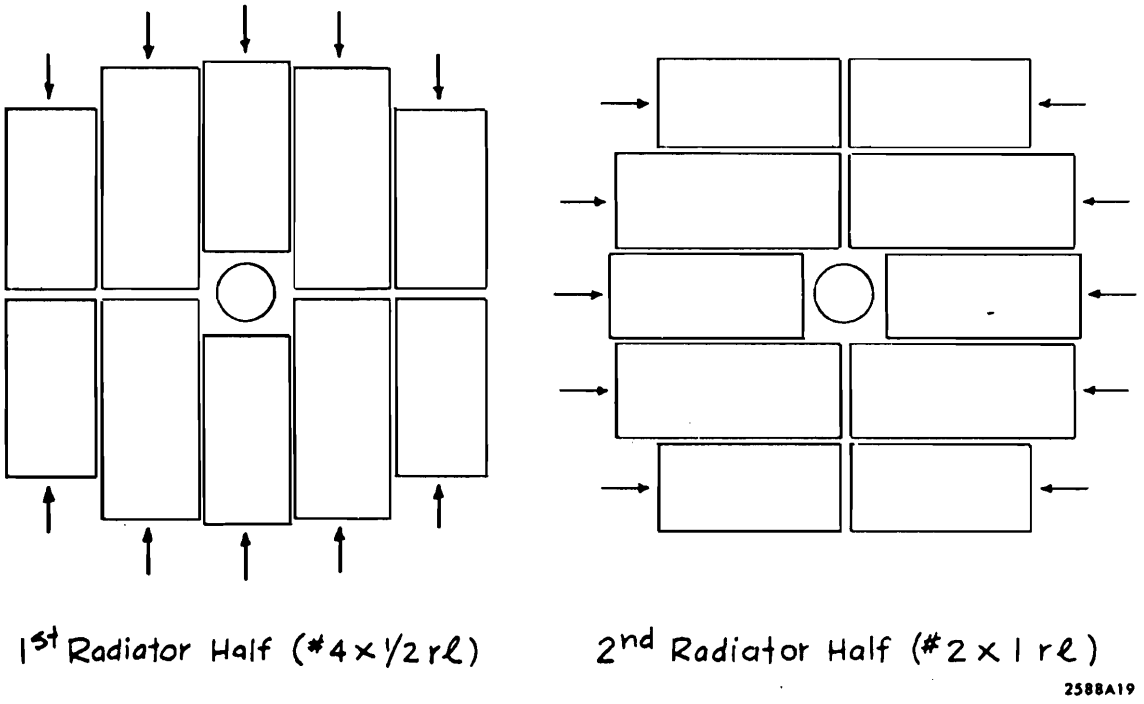

Fig. I-3

A possible end section assembly.

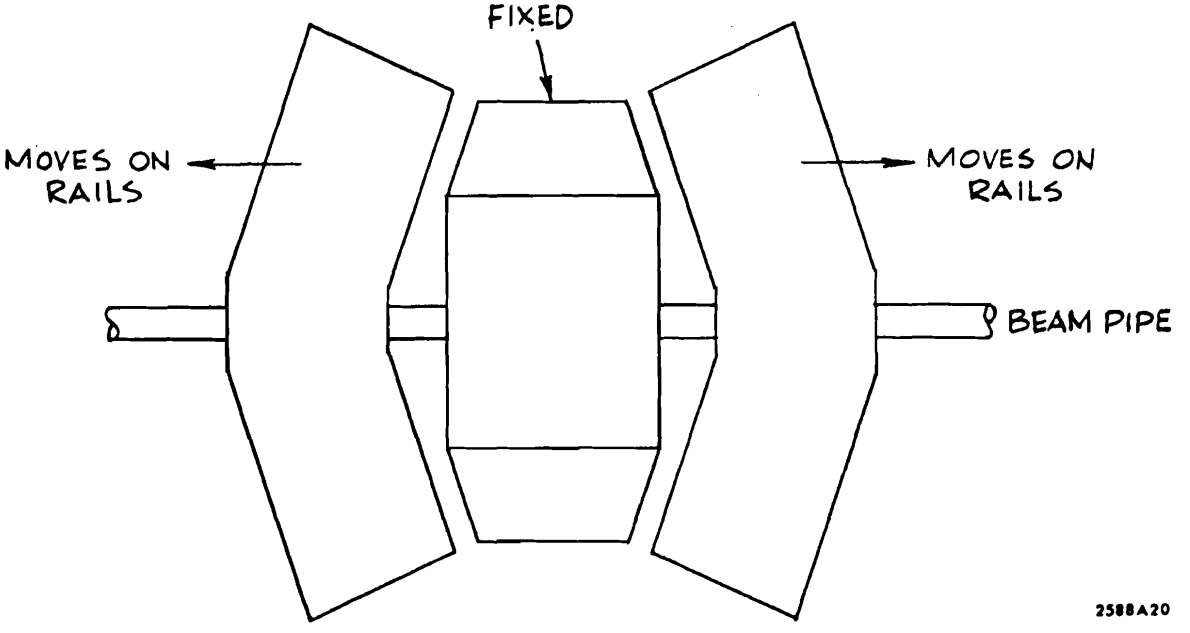

Fig. I-4

A schematic diagram showing the moveable end sections.